University of Kerbala

College of Science

Department of Physics

Polyimide Structural and Non - Linear Optical Properties Investigation Utilizing the Density Functional Theory

A thesis Submitted to the Council of the College of Science, University of Kerbala in Partial Fulfillment of the Requirements for the Master Degree of Science in Physics

By

Zainab Adil Ahmad

B.Sc. University of Kerbala 2011

Supervised by

Dr. Qasim Hassan Ubaid   **Assist. Prof Dr. Mohammed A. Alkaabi**

2024 A.D.   1446 A.H.

بسم الله الرحمن الرحيم

ذَلِكَ فَضْلُ اللَّهِ يُؤْتِيهِ مَن يَشَاءُ وَاللَّهُ ذُو الْفَضْلِ الْعَظِيمِ

صدق الله العلي العظيم

سورة الجمعة: الآية ٤

Supervisor Certificate

We certify that the thesis entitled " *Polyimide Structural and Non Linear Optical Properties Investigation Utilizing the Density Functional Theory* "was prepared under our supervision by *(Zainab Adil Ahmad)* at the Science College/ Kerbala University as a partial fulfilment of the requirements for the master degree of Science in Physics.

Signature:

Name: **Dr. Qasim Hassan Ubaid**

Title: Lecturer

Address: Department of Physics, College of Science/University of Kerbala

Signature:

M. A. AL-KAAB

Name: **Dr. Mohammed Abdulhussain AL-Kaabi**

Title: Assistant Professor

Address: Department of Physics, College of Science/University of Kerbala

Date: /   / 2024

In view of the available recommendations, I forward this thesis for debate by the examining committee.

Signature :   N. A. AL-KAABC

Name :**Dr. Mohammed Abdulhussain AL-Kaabi**

Title: Assistant Professor

Head of the Department of Physics, College of Science/ University of Kerbala

Date: 11/ 9 / 2024

Examination Committee Certification

We certify that we have read this thesis, entitled " *Polyimide Structural and Non Linear Optical Properties Investigation Utilizing the Density Functional Theory* " and as an examining committee, examined the student " *Zainab Adil Ahmad* " on its contents and that in our opinion it is adequate for the partial fulfillment of the requirements for the Master Degree of Science in Physics.

Signature:

Name: **Dr. Rajaa K. Mohammad**

Title: Professor

Address: University of Kerbala,

College of Science, Department of Physics.

Date: /   / 2024

(Chairman)

Signature:

Name: **Dr. Nidhal M. Alshareefi**

Title: Assist Professor

Address: University of Babylon,

College of Science, Department of Physics.

Date: 15/9/2024

(Member)

Signature:

M.A-AL-KAABi

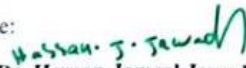Name: **Dr. Mohammed A. Al-Kaabi**

Title: Assist Professor

Address: University of Kerbala,

College of Science, Department of Physics.

Date: 18/9/2024

(Member & Supervisor)

Signature:

Hassan. J. Jawad

Name: **Dr. Hassan Jameel Jawad AL-Fatlawy**

Title: Professor

Address: **Dean of the College of Science, University of Kerbala**

Date: /   /

Signature:

Name: **Dr. Nibras M. Umran**

Title: Professor

Address: University of Kerbala,

College of Science, Department of Physics.

Date: /   /

(Member)

Signature:

Name: **Dr. Qasim H. Ubaid**

Title: Lecturer

Address: University of Kerbala

College of Science, Department of Physics.

Date: /   /

(Member & Supervisor)

Dedication

-To the refuge to which those seeking help resort, and to the light by which we are guided. The greatest Prophet Muhammad and his pure family.

- To the soul of my beloved, my dear father .

- To my dear mother.

- To my support in this life is my husband.

- To my children.

-To everyone who helped and supported me.

Acknowledgment

I am most grateful to Allah Almighty for giving me the chance to fulfil this dream .

I would like to thank my supervisors for their support and encouragement Assist. Prof Dr. Mohammed A. Alkaabi and Dr. Qasim Hassan Ubaid with their advice, encouragement, and support while I was studying .

I express my gratitude to the Dean of the College of Science, the President of the Physics Department, and each one of the Physics Department's faculty members .

My sincere gratitude and thanks to my mother and husband for their unwavering support during the study period.

Zainab Adil

Abstract

In this study, density functional theory (DFT) calculations were performed to investigate the structural, nonlinear optical (NLO), and spectroscopy properties for the pristine Polyimide (PI) monomer. The potential energy surface (PES) scan was performed using the semi-empirical method PM6 to predict the best conformer. The B3LYP functional, which employs Beck's three-parameters hybrid exchange functional and the Lee-Yang-Parr correlation functional, and 6-311G(d,p) were used effectively to optimize the monomer and assess the properties. The calculated average value of bond lengths was found to be 1.392 in Angstrom units, while the average value of the bond angles was 119.8 in Degree units. The bond lengths and bond angles from DFT were in good agreement with the experimental data.

The charge distribution by natural bond orbitals (NBO) methode, and NLO properties as dipole moment, polarizability, first-order hyperpolarizability, and susceptibility were also studied. The observation of an uneven distribution of charges led to a non-zero dipole moment of 1.52 Debye.

Finally, the infrared spectrum was obtained and examined after being adjusted by a scaling factor of 0.9679. The UV absorption spectrum was investigated using the TD-B3LYP method with the same basis set. The maximum wavelength at the oscillator strength (f = 0.0007) was found to be 513 nm, which is in good agreement with the experimental value of 500 nm.

Table of contents

List of Figures

List of Tables

List of Symbols

PMDA	Dianhydride monomer
ODA	Diamine monomer
PAA	Polyamic acid
H	Hamiltonian operator
PI	Polyimide
M_I	Nucleus mass
m_i	Electron mass
$T[\rho]$	Kinetic energy of non-interacting system
$E_{ne}[\rho]$	External energy
$E[\rho]$	Total energy
$J[\rho]$	Electron-Electron repulsion energy
$T[\rho]$	Kinetic energy of non-interacting system
V_{NN}	potential energy operator of nuclei- nuclei
V_H	Hartree potential
r_{ij}	Distance between electron i and j
N_n	Normalization factor
N	Atomic count
$\rho(r)$	Electron density
V_{ext}	External potential
V_{ion}	Nuclei potential
r_{Ii}	Distance between nuclei I and electron i
n^*	Active main quantum number
V_{XC}	Exchange-correlation potential
E_{XC}	Exchange - correlation energy

ζ	Orbital exponent
μ	Dipole moment
α	Polarizability
β	First order hyperpolarizability
α'	Polarizability volume
χ	Susceptibility
ψ	Wavefunction
$\boldsymbol{\alpha}$	Spin up of electron
$\boldsymbol{\beta}$	Spin down of electron
Ψ_i	Spatial wave function
η	Reduced mass
$_A N$	Avogadro's number
$R_{nl}(r)$	Radial part of the atomic functions for STOs
$(\theta, \Phi) Y_{lm}$	pherical harmonic of the atomic functions for STOs
NDDO	Neglect of Diatomic Differential Overlap
MO	Molecular orbital
AM1	Austin model 1
PM3	Parametric Model number 3
PM6	Parametric Model number 6
HF	Hartree Fock
URHF	Unrestricted Hartree-Fock
RHF	Restricted Hartree Fock
DFT	Density Functional Theory
HK	Hohenberg-Kohn
LDA	Local density approximation
LSDA	local spin-density approximation

GGA	Generalized gradient approximation
LCAO	Linear combination of atomic orbitals
STO	Slater-type orbitals
GTO	Gaussian-type orbitals
PES	Potential energy surface
FT-IR	Fourier transform Infrared spectroscopy
B3LYP	Beckes three parameter hybrid functional with lee-yang-Parr correlation functional

Chapter One

Chapter One
General Overview and Litrature Review

1.1 Introduction

Since the dawn of time, polymers have existed as the fundamental building blocks of all life. Every class of living thing is composed of polymers. However, our comprehensive understanding of the true nature of polymers did not begin to develop until the middle of the 20th century. The discovery of plastics, genuine man-made materials and the pinnacle of human ingenuity and creativity, played a crucial role in this development [1].

Polymers are large, long-chain molecules with a high molecular weight [2]. These are massive particles composed of units that repeat chemically and are connected like beads. Each series typically contains more than five monomers, but some may contain hundreds or thousands of monomers [3]. The field of polymer science has advanced to an extremely high degree of sophistication. Synthetic polymers with precisely defined molecular weights and comparatively simple property designs are now attainable [4].

1.2 Polyimide (PI)

1.2.1 Structure of Polyimide

The PI monomer (PI, $C_{22}H_{10}O_5N_2$) [5] is produced by two-step:

The First step: Involves synthesizing polyamic acid (PAA) from dianhydride (PMDA) and diamine monomers (ODA) using an exothermic polycon densation reaction in a dipolar solvent.

The Second step: Involves applying an imidization reaction after PAA has been solvent-eliminated. See Figure 1.1.
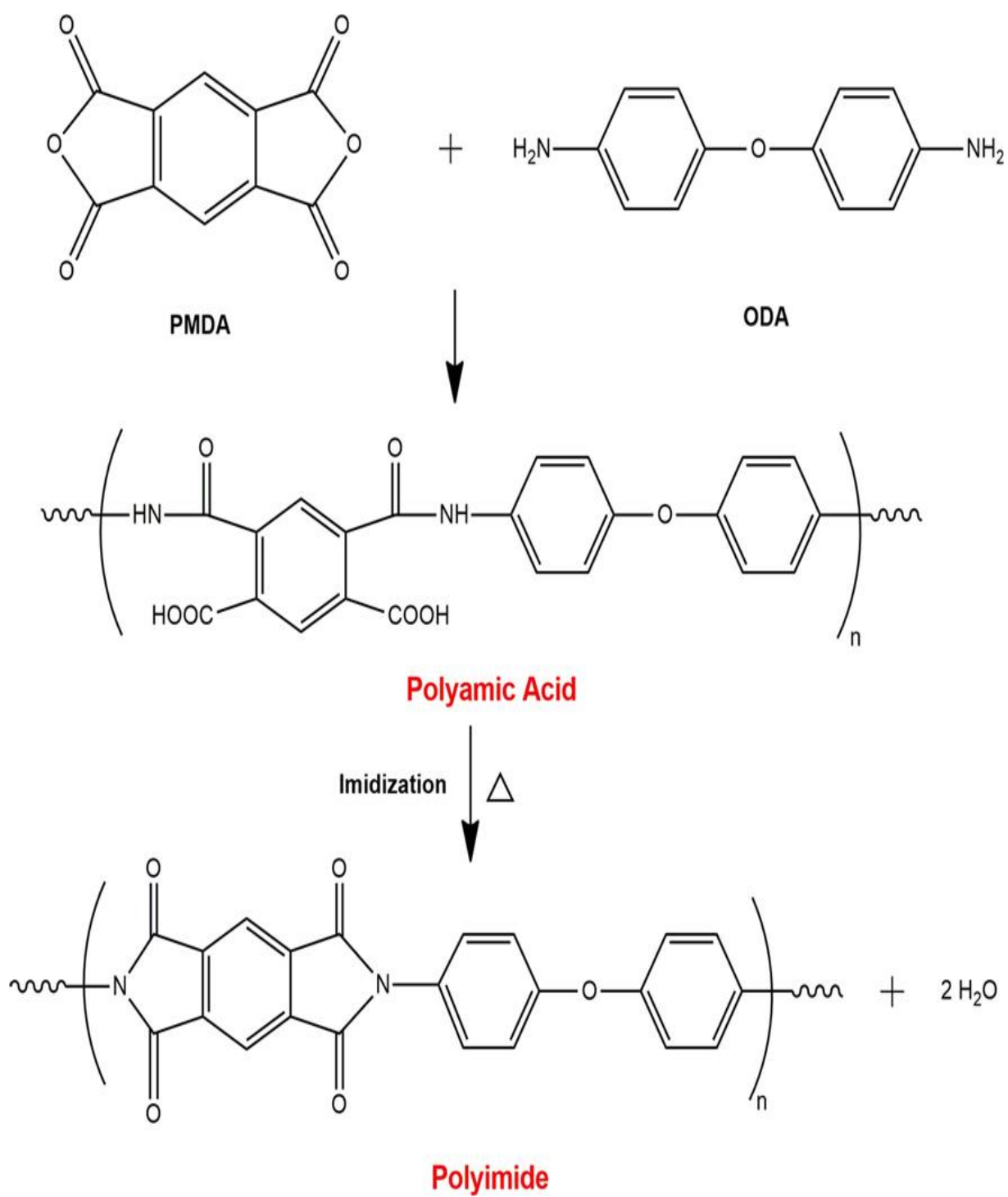
Figure 1.1: Synthesis mechanism of PI [6].

1.2.2 Properties of Polyimide

Marston Bogert initially created aromatic polyimides (Kapton: The Commercial Name) in 1908 [7]. The polymer chain of heterocyclic compounds, featuring a ring structure identified as polyimide, was first documented in 1955 by Robison and Edwardas patent [8]. Polyimides have drawn more interest because of their thermal and chemical durability, low dielectric constant, high electrical resistivity, and relative simplicity in the production of coatings and films [9]. Moreover, PIs have thermal stability, making them an excellent choice for the manufacture of flexible sensors [10-14]. PI films are employed in these applications as a substrates, electrical insulators. However, this substance has a smooth surface and is chemically inert. Hence, particular surface treatments are needed for their optimal adherence to other materials [15-17]. However, the majority of conventional polyimide films typically exhibit strong colouration, ranging from deep yellow to brown. This significantly restricts their use as transparent, flexible substrates in the fields of solar cells, displays, and lighting [18-20]. Table 1.1 shows the physicochemical properties of PI.

Table 1.1: Physicochemical properties of PI [21].

Property	Unit	Polyimide
Thickness	μm	5.963
Density	g/cm^3	1.4000
Refractive index	-	1.696
Dielectric constant	-	2.878
Color	-	Orange\yellow
Fractional free volume	-	0.3167

1.2.3 Applications of Polyimide

1.2.3.1 Sensor Applications

Optical fibers find application in laser systems, medical diagnosis devices, sensors, and instrumental analysis devices in chemistry. Because these fibers carry out vital missions, embedded optical components must have mechanical durability, functional lifetime, and resistance to process conditions. To provide high temperature resistance up to 400 °C as well as mechanical strength such as high modulus and abrasion resistance, the cladding is coated with fragile PI film (5–10 μm) [6, 22-25].

1.2.3.2 Electronic Devices and Battery Applications

Due to the PI excellent dielectric qualities, which include high electrical insulation (dielectric constant 3.4–3.5), high flexibility, and low thermal expansion coefficient, PIs are ideal for use in electronic applications [26-28]. Under operating conditions, electronic displays exhibit thermal shrinkage problems [29]. Adding PIs as microelectric coatings improves thermal stability and mechanical strength [30].

1.2.3.3 Membrane Applications

Because of their porous structure, membranes are preferred for separation applications like liquid evaporation [31], gas separation [32], water treatment [33], and so on. The PI coating on the membrane structure can improve the membrane's resistance to heat and chemicals [29, 34].

1.2.3.4 Anticorrosion Applications

Polymeric coatings prevent corrosion by physically preventing species like H^+ and O_2 from diffusing [35]. NASA created a new PI powder coating material with anti-corrosion properties for metal substrates like

pipes and other infrastructure parts, machinery, exposed metal parts and structures, car components, and bridges [36].

1.2.3.5 Capillary Tubes

The capillary tubes in column chromatography devices are notably fragile, susceptible to elevated temperatures, and degrade in quality with prolonged chemical use. This compromises the reliability of the device. In practical applications, capillary columns benefit from flexible polymers that exhibit strong adhesion, mechanical flexibility, resilience to abrasion and bending, and chemical resistance. Polyimide (PI) emerges as an optimal choice for a high-performance coating material possessing these essential qualities [37].

1.2.3.6 Metallic Substrates

Due to their cost-effectiveness and excellent electrical and thermal conductivity, copper materials find frequent use in electronic devices. However, as copper can undergo oxidation under high temperatures or in high humidity conditions, protective coatings become essential to enhance the reliability and lifespan of the materials. Applying a polyimide (PI) coating is a viable method to mitigate these detrimental effects [6]. Some applications of PI are shown in Figure 1.2.
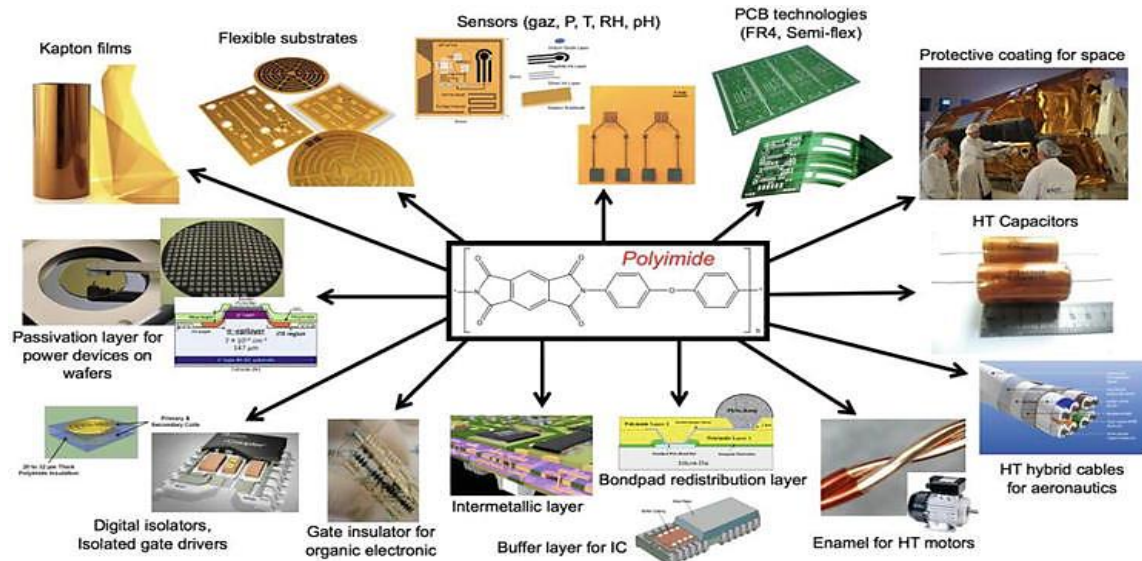
Figure 1.2: Overview of the main electronic and engineering industrial applications of PI [38].

1.3 Previous Studies

Below are some studies that done for the polyimide, encompassing both theoretical and experimental approaches:

Takahashi et al. (1984) [39] obtained PI by heating poly (amic acid) PAA films. Where it was determined through wide-angle X-ray diffraction analyses. According to the results, the condensed states of PAA chains showed a high molecular order that is similar to that of a liquid crystalline state. In addition, bond length and bond angle values are found.

Ramos et al. (1993) [40] studied theoretically the effects of chemical bonding on the adhesion of both aluminium atoms to the polyimide surface and PI deposited on the surface, within a cluster model framework. Furthermore, they examined and contrasted the experimental values of PMDA-ODA's bond lengths and bond angles. The comparison between the two approaches suggests that the PI geometry using Completely Neglects the Differential Overlap (CNDO) approximation could provide reliable experimental data.

Diaham et al. (2011) [41] investigated the impact of imidization temperature on the molecular structure, thermal, and electrical properties of PI thin films. They used Fourier transform infrared (FTIR) spectroscopy to assess imidization effects. As a result, the amide and imide peaks in FTIR spectra can only be identified by assigning the absorption bands to the detected chemical bond changes during the imidization of PAA into PI. Additionally displayed the typical absorption vibrational modes for PI and PAA.

Abe Atsutoshi et al. (2011) [42] analyzed the theoretical PI coloration mechanism. They employed the long-range-corrected time-dependent density functional theory (TDDFT) within the B3LYP method and 6-31G(d) basis sets to compute oscillator strengths and excitation energies. The result appeared to indicate a significant influence of intermolecular interaction on coloration. Furthermore, the coloration is also influenced by the molecular orbitals restless by the intermolecular interaction. By combining the results of electronic structure calculations using TDDFT and MD simulations with experimental data, they were able to shed light on the mechanism underlying PI coloration.

Lyulin et al. (2013) [43] utilized atomic-scale, microsecond molecular dynamics simulations MD to gain an understanding of the thermal and structural characteristics of heat-resistant polyimides. They proved that the degree of equilibration has little effect on the macroscopic properties of a polyimide sample, such as density and the glass transition temperature. Ultimately, it was discovered that electrostatic interactions had a significant impact on the characteristics of the heat-resistant polyimides. Specifically, when intra- and intermolecular dipole interactions are present, individual polymer coils become compacted,

leading to an increase in the glass transition temperature and polymer density.

Umar et al. (2015) [44] presented a detailed vibrational assignment of terephthaloyl chloride based on potential energy distribution based on experimental FTIR recordings. Structure properties and vibrational wavenumbers of the equilibrium geometry were calculated using the DFT/B3LYP with the standard basis set 6-311++G (d,p). The experimental FTIR wavenumbers and the scaled vibrational wavenumbers agree well. Overall, anticipated that this study's findings will be crucial to comprehending this molecule's dynamics.

Atta et al. (2015) [45] presented the exposure of polyimide films to oxygen plasma and how it affects the PI's physical properties. They discovered that the PI was semi-crystalline by using X-ray diffraction (XRD) to analyze the sample's structure. Their study included using thermo gravimetric analysis (TGA) to show that at various time intervals (between one and five minutes) exposure to oxygen plasma could enhance the thermal stability of polyimide films. Moreover, they calculated the optical constants like the complex dielectric constant (K) and refractive index (n). It was observed that the fundamental optical constants were highly dependent on the exposure time. There was a decrease in the refractive index after being exposed to oxygen plasma.

Mikšová et al. (2016) [46] studied ion irradiation's effect on PI Through several techniques, including XRD and UV-Vis. They discussed how the different ion species used in the irradiation affect the structural alterations and PI modification. It has been demonstrated that the ion flux and the chemical structure of the polymer determine the changes brought about by radiation. An increase in the number of carbon atoms per cluster is caused by a slight decrease in the hydrogen concentration in PI. XRD

measurements have shown variations in PI's crystal. The modification of PI by heavy ions has little effect on the experimentally determined ion-energy losses and energy straggling due to PI's strong resistance to radiation degradation.

Nam Ki-Ho et al. (2017) [47] computed the thermomechanical properties of the model poly(ester imide)s (PEsIs) via the MD method. Bond stretching and angular variation were found to have the greatest impact on the coefficient of thermal expansion (CTE). The optical and thermo-mechanical behaviors of the polymer are significantly influenced by the dimethyl groups in its backbone structure. The outcomes they reached of the MD simulations were in good agreement with the experimental findings.

Ando Shinji et al. (2018) [48] examined the behaviors of thermally cross-linkable polyimide (PI) films with isomeric diamine structures in order to lower the polymer films' coefficient of volumetric thermal expansion (CVE). DFT/B3LYP was used with 6-311G+ (2d, p) as a basis set to calculate the polarizability in mid- and far-IR vibrations and a 6-311G (d, p) basis set for geometry optimization. The calculation for far-IR spectra and the experimental spectra resemble each other. Suppressing the intermolecular free volume expansion and local molecular motions, which appear at high temperatures. One efficient way to lower the CVE of aromatic polymers was the integration of crosslinking reactions into the main chain.

Rahnamoun et al. (2019) [49] used reactive molecular dynamics simulation, along with the polarizable ReaxFF method, to model the irradiation of polymers by highly energetic electrons. As well as they studied the effect of electron irradiation on the breaking of intermolecular bonds and the creation of free radicals in Kapton polyimide. Their results

showed that hydrogen atoms split off from various places within the polyimide during irradiation by an electron beam. Also the breaking of the chemical bonds, the formation of new bonds, and changes in the polyimide material.

Yang et al. (2021) [50] used amorphous models of polyamide 66 (PA66), polyamide 6T (PA6T), and Benz imidazole (PPTA) to study the effect of chain rigidity on intermolecular H-bonds and the mechanism of forming free H-bonding. The study was conducted using MD simulation in conjunction with DFT/B3LYP calculations and a 6-31G (d,p) basis set. It has been discovered that, because of PPTA's relatively weak conformational adjustment, there are a lot of free H-bonding sites. Through the development of stronger interchange H-bonding interactions. This study provides a better understanding of the relationship between chain behavior and intermolecular H-bonds in rigid chain polymers and offers a novel way to improve their performance.

Lei et al. (2022) [51] analyzed the dielectric constant of linear aromatic polyimides by using various calculation techniques. They used a combination of molecular dynamic simulation (MD) and density functional theory (DFT) could yield accurate prediction results. The optimal combination of functional and basis sets to predict the dielectric constant using MD simulation are 6-311++g (d,p) and CAM-B3LYP. However, the dipole fluctuation formula takes a longer time (>10 ns) to converge, which results in higher computing costs. The results served as the foundation for creating a workable database that will allow the structure information of aromatic polymers, such as polyimides, to be correlated with their dielectric properties. This will shorten the time and price of polymer discovery experiments and speed up the process of creating low-dielectric-constant polymer materials.

Tan et al. (2023) [52] studied a novel diamine (DPPTPDA) with a chromophore based on TDPP. After that, DPPTPDA was polymerized with Pyromellitic dianhydride (PMDA) to produce an intrinsic black polyimide BPI (DPPTPPI). DPPTPPI has good electrical performance and a low coefficient of thermal expansion. High solder heat resistance and peel strength are demonstrated by the flexible copper-clad laminate based on DPPTPPI films. The study offered theoretical guidance for designing high-performing intrinsic BPI materials at the molecular level with an eye toward real-world microelectronic applications.

Raluca et al. (2023) [53] compared the effects of dianhydride on specific physical properties that are relevant to display applications between a fully aliphatic and semi-aromatic polyimide (PI). Molecular modelling results demonstrated that the unique conformational characteristics of PI have an impact on how the polymer interacts with molecules. Furthermore, Molecular modelling revealed that the interaction is softly impacted by the dianhydride unit's unique flexibility and polarizability. When charge-transfer complex (CTC) interactions are low, optical transmittance increases. Optical studies showed varying degrees of transparency depending on the sample structure's aromatic extent.

Luo et al. (2023) [54] computed the van der Waals volume, dipolar moment, polarizability, and electrostatic potential surface for a range of ester-containing polyimides (EPIs). The study was conducted using molecular dynamics (MD) and the DFT/B3LYP method within the 6-31G(d)basis sets. The findings suggested that there is a strong correlation between dielectric permittivity and the dipolar moment density. The cause is that the dominant polarization mode in ester-containing polyimides is dipolar polarization.

1.4 The Aim of the Work

This thesis aims to theoretically investigate the structural properties of polyimides using the hybrid method B3LYP in density functional theory with a basis set of 6-311G (d, p). The primary objective is to predict properties such as bond length, dihedral angle, bond angle, and total energy. Additionally, inspect the non-linear optical characteristics like dipole moment, polarizability and hyperpolarizability, natural atomic charge distribution, and optical susceptibility. Gaussian 09 software is used for all calculations, and GaussView06 is used to visualize and analyze the results. Furthermore, exploring the PI spectroscopy properties depending on vibrational frequencies, such as ultraviolet (UV) and infrared (IR) spectroscopy.

Chapter Two

Chapter Two
Evolution of Quantum Computational Methods

2.1 Introduction

This chapter provides an overview of the theories and computational techniques that are used to study the structure and nonlinear optical properties of molecules. One of the most well-known and commonly used theories is the density functional theory (DFT), which considers the electronic structure and interactions within a molecule. DFT is widely applied in ab-initio molecular dynamics, allowing for the computation of quantum states in atoms, molecules, and solids. The chapter also includes explanations of various programs and basis set types utilized in these computational studies. Furthermore, it delves into the Schrödinger equation, a fundamental equation in quantum mechanics that describes the behavior of particles at the atomic and molecular levels. Molecular computing techniques and their applications are also discussed, along with an exploration of nonlinear optical properties.

Finally, the chapter concludes with an overview of the methods employed to investigate vibrational properties.

2.2 Schrodinger Equation

A system of interacting particles has energy E, which is equal to the sum of its potential energy function V and kinetic energy contribution T, according to classical mechanics [55]:

$$E = T + V \tag{2-1}$$

Schrodinger introduced the full mathematical underpinnings of non-relativistic quantum mechanics in 1926 [56]. The fundamental equation

of quantum theory is the Schrodinger equation. In current physics, the study of these equations is critically important [57].

$$\hat{H}\,\psi = \hat{E}\,\psi \qquad (2\text{-}2)$$

Where the energy is $\hat{E}$, and the wavefunction is ψ. The kinetic energy and potential energy operators make up the Hamiltonian operator H. For simplicity, we use a 1D notation and express the operator in the coordinate representation as [58]:

$$H \;=\; T \,+\, V \;=\; -\frac{\hbar^2\,\partial^2}{2m\partial x^2} + V(x) \qquad (2\text{-}3)$$

The nuclei and electrons that make up the molecular Hamiltonian through the static Coulomb potential, electrons and nuclei interact expressed as follows [59] :

$$\hat{H} = \hat{T}_N(R) + \hat{T}_e(r) + \hat{V}_{eN}(r,R) + \hat{V}_{NN}(R) + \hat{V}_{ee}(r) \qquad (2\text{-}4)$$

The electronic and nuclear motions are typically addressed independently since electrons are substantially lighter than nuclei.

$\hat{T}_N(R)$ and $\hat{T}_e(r)$ are the kinetic energy operators of nuclei and electrons, respectively. $\hat{V}_{eN}(r,R)$, $\hat{V}_{ee}(r)$, and $\widehat{V}_{NN}(R)$ are the potential energy operators for electron-nuclei, electron-electron, and nuclei-nuclei, respectively. Whereas r denotes electron coordinates, R stands for nuclear coordinates. Consequently, equation (2-4) can be written as [60]:

$$\hat{H} = -\frac{\hbar^2}{2}\sum_{I=1}^{N}\frac{\nabla_I^2}{M_I} - \frac{\hbar^2}{2}\sum_{i=1}^{n}\frac{\nabla_i^2}{m_i} + \sum_{I=1}^{N-1}\sum_{i=1}^{n}\frac{e\,Z_I}{r_{Ii}} + \sum_{I=1}^{N-1}\sum_{J=I+1}^{N}\frac{Z_I Z_J}{R_{IJ}}$$

$$+ \sum_{i=1}^{n-1}\sum_{j=i+1}^{n}\frac{e^2}{r_{ij}} \qquad (2\text{-}5)$$

Where ∇_I^2 is the electron's Laplacian operator for nucleus , ∇_i^2 is the electron's Laplacian operator for electron, Z_I and Z_J are the charges of the nuclei of atoms I and J, r_{Ii} is the distance between nuclei I and

electron i, R_{IJ} is the distance between nuclei I and J, and r_{ij} is the distance between electrons i and j. Other variables include: M is the mass for the nucleus, m, e are the mass, and charge for the electron, respectively. The Schrodinger equation shows that the energy function consists of three terms: the electron-electron interaction, the interaction with the external potential, and the kinetic energy.

The generality of the Schrodinger equation and the Hamiltonian has a drawback: even in basic systems like the hydrogen atom, we are unable to pinpoint the precise location of any electron. The location of the electron must fit into a probability distribution that is controlled by a function known as the wavefunction.

 For the majority of systems, the Schrodinger equation cannot be solved in closed form. Furthermore, only a few simple systems have exact solutions for the wavefunction and energy E. We have to accept approximations for solutions in most cases [61].

The Hamiltonian operator (in atomic units, e^2 and $\hbar^2$=1) can be expressed as follows with these approximations:

$$\hat{H} = -\frac{1}{2}\sum_{I=1}^{N}\frac{\nabla_I^2}{M_I} - \frac{1}{2}\sum_{i=1}^{n}\frac{\nabla_i^2}{m_i} - \sum_{I=1}^{N-1}\sum_{i=1}^{n}\frac{Z_I}{r_{Ii}} + \sum_{I=1}^{N-1}\sum_{J=I+1}^{N}\frac{Z_I Z_I}{R_{IJ}} +$$

$$\sum_{i=1}^{n-1}\sum_{j=i+1}^{n}\frac{1}{r_{ij}} \tag{2-6}$$

2.3 The Approximations Methodologies for Quantum Computations

Since Schrodinger's equation cannot be precisely solved by analytical methods for more than two particles, approximate methods are used to predict the structure of all atoms or molecules.

❖ Molecular Mechanics Method (MM).

❖ Semi-Empirical Method (SE).

❖ Ab -initio calculation.

2.3.1 Molecular Mechanics Method (MM)

Predicting the specific physical characteristics and structure of molecules could be the aim of molecular mechanics [62]. Entropies, strain energies, dipole moments, and enthalpies of formation are a few examples of physical attributes that can be computed. Molecular Mechanics (MM) determines a molecule's energy and then modifies it by varying bond lengths and angles to produce the least possible energy structure [62]. MM ignores electrons and assumes that molecules are balls held together by springs. Following the creation of small- to medium-sized molecule energies and geometries modeling polymers is the primary application of MM. Additionally, applicable to big molecules like enzymes, they can act as quantum mechanical input structures [63]. These approaches are entirely empirical, ignoring any consideration of electrons in favor of applying the principles of classical physics. They also require experimental data on parameters. Because the MM method computes more quickly than the other methods, it can be applied to processes like conformational energy searching and molecular dynamics [64].

2.3.2 Semi-Empirical (SE) Method

Electronic structure theory can be simplified to semi-empirical methods. They are usually 1000 times faster than DFT treatments, but they are also less accurate and robust overall. However, in contrast to classical force fields, they can handle electronic events like chemical reactions and electronic excitations that cannot be described at the MM level, despite being several orders of magnitude slower than MM

treatments. Semi-empirical techniques bridge the gap between DFT and classical force fields, allowing for practical electronic structure calculations on large complex systems in all areas of chemistry with a reasonable degree of accuracy. They are helpful tools in theoretical studies of large molecules, especially when used practically in a multi-method strategy [11]. The fundamental Neglect of Diatomic Differential Overlap (NDDO) approximations were developed by Pople and then significantly altered by Dewar and Thiel [65]. The most popular and widely used approaches for analyzing ground-state potential surfaces are the Parameterization Method (PM3) [66], the Modified Neglect of Differential Overlap (MNDO) [67], and the Austin Method Version (AM1) [68].

2.3.3 Ab-Initio Style

The goal of the majority of ab initio or first-principles methods based on basic quantum theory is to compute the electronic structure or stationary states of electrons in the atomic nuclei's electrostatic field. The ground state's energy can then be used to investigate the nuclei's displacements, resulting in the determination of numerous macroscopic properties that are crucial to technology.

The primary benefit of the ab initio method is its independence from experimental data; instead, it uses a variety of approximations to solve Schrödinger's equation. This method describes atomic orbitals using wave functions, which are then used to calculate molecular properties, as opposed to semi-empirical techniques [69]. Therefore, ab initio methods can also be applied to the computation of certain structural and mechanical properties of hypothetical systems, for example, to the prediction of properties of as-yet-undeveloped materials [70]. The number of atomic orbitals and basis set quality can affect the quality of

the molecular orbitals used and, therefore, the precision of the calculated molecular properties. The correlation between the electrons' motions is frequently ignored by electronic energy [71]. For small and medium-sized systems, ab initio methods are the most dependable, but they take an excessive amount of time for larger systems [72].

2.4 Approximation of Born-Oppenheimer (BO)

Born and Oppenheimer developed the Born-Oppenheimer approximation in 1927. Both nuclei and electrons are present in molecules, but since the nuclei are much heavier than the electrons, led to constrained on their motion. Ultimately, the nuclear and electronic motions can be dealt with independently. Therefore, the nuclear kinetic energy can be disregarded when resolving the electronic problem [73]. We refer to the Born-Oppenheimer approximation as the isolate of nuclear and electronic motion [56].

$$\hat{H} \approx \hat{H}_n + \hat{H}_e \tag{2-7}$$

$$\Psi(r_1, r_2, \dots, r_N, R_1, R_2, \dots R_M) \approx \Psi_n(R_1, R_2, \dots R_M)\Psi_e(r_1, r_2, \dots, r_N) \tag{2-8}$$

$$E \approx E_n + E_e \tag{2-9}$$

By relying on the Schrödinger equation (2-2). Therefore, Schrödinger equations can be divided into one electronic and the other nuclear:

$$\hat{H}_n\Psi_n(R_1, R_2, \dots R_M) = E_n\Psi(R_1, R_2, \dots R_M) \tag{2-10}$$

$$\hat{H}_e\Psi_e(r_1, r_2, \dots r_N) = E_e\Psi(r_1, r_2, \dots r_N) \tag{2-11}$$

The electronic Hamiltonian can be written as:

$$\hat{H}_{elec} = -\sum_{i=1}^{N} \frac{1}{2}\nabla_i^2 - \sum_{A=1}^{M}\sum_{i=1}^{N} \frac{Z_A}{r_{iA}} + \sum_{i=1}^{N}\sum_{j>i}^{N} \frac{1}{r_{ij}} \tag{2-12}$$

The nuclear Hamiltonian is [74]:

$$\hat{H}_{nucl} = -\sum_{A=1}^{M} \frac{1}{2M}\nabla_A^2 + \sum_{A=1}^{M}\sum_{B>A}^{M} \frac{Z_A Z_B}{R_{AB}} \tag{2-13}$$

The nuclear kinetic energy operator has been ignored, but the equation still contains the internuclear repulsion terms, which are known from the nuclear charges and internuclear distances. The equation includes terms for potential energy resulting from attractive forces between nuclei and electrons as well as terms for potential energy resulting from repulsive forces among electrons. Almost all calculations of molecular orbitals and the majority of calculations of atomic energy use the Born-Oppenheimer approximation. Because the approximated energies closely resemble the energies found in test cases on straightforward systems where the approximation is not made, it is a very good approximation [61].

2.5 Hartree (H) Approximation

The Schrodinger equations need to be calculated independently and consistently concerning the wavefunctions of the other electrons. A quantum multi-electron system in a stationary state can have its wave function and energy approximated using the Hartree method. It is assumed that the wavefunction in the Hartree approximation is a product of one-particle wave functions. There is no anti-symmetry in the wavefunction [75]. Also believed that the overall wavefunction of an n-electron system could be expressed as a product of the functions of individual electrons $\psi_1, \psi_2, \dots, \psi_n$.

$$\psi(1,2,\dots,n) = \psi_1(1)\psi_2(2)\psi_3(3)\dots\dots\psi_n(n) \tag{2-14}$$

Unfortunately, Hartree approximation violates the Pauli Exclusion Principle, which states that two electrons cannot be described by the same four quantum numbers. The wave function only needs to be anti-symmetric for the Pauli Exclusion Principle to apply to electrons [76].

2.6 Hartree–Fock (HF) Approximation

The one-electron approximation, which uses a single-particle Schrodinger equation to describe an electron's motion in the effective field of all other electrons, is the foundation of the Hartree-Fock self-consistent method. The Hartree-Fock approximation accounts for the correlation that results from electrons with the same spin; however, it does not account for the uncorrelated motion of electrons with the opposite spin [62]. The Hartree-Fock equations provide an improvement of 10–20% when compared to the Hartree equations because the energy has been reduced by the exchange term. The self-consistent-field (SCF) method is used to solve the Hartree-Fock equation. As a result, in addition to meeting the Schrodinger equation, the exact wave function also needs to be anti-symmetric. This last requirement can be simply met by applying slater determinants [77]. The Slater determinant states that the wave function of a system with N electrons is expressed as follows:

$$\psi(\mathrm{r}_1, \mathrm{r}_2, \ldots, \mathrm{r}_N) = \frac{1}{\sqrt{N!}} \begin{vmatrix} \psi_1(r_1) & \psi_2(r_1) & \ldots & \psi_N(r_1) \\ \psi_1(r_2) & \psi_2(r_2) & \ldots & \psi_N(r_2) \\ \vdots & \vdots & & \vdots \\ \psi_1(\mathrm{r}_N) & \psi_2(\mathrm{r}_N) & \ldots & \psi_N(\mathrm{r}_N) \end{vmatrix} \qquad (2\text{-}15)$$

The data is normalized using the factor $\frac{1}{\sqrt{N!}}$. This method can be used to solve the Schrödinger equation for a quantum system with n electrons and N nucleus, where ψ is the spin-orbit electronic wavefunction.

This determinant describes how the spin of electrons follows Pauli's exclusion principle. The spin up (α) and spin down (β) values of the electrons are $(+\frac{1}{2})$ and $(-\frac{1}{2})$, respectively.

❖ Restricted Hartree-Fock Method (RHF)

The way in which orbitals are constructed to reveal paired or unpaired electrons is a variant of the HF method. If the molecule has a singlet spin, the same orbital spatial function can be applied to both α and β spin electrons in each pair [78].

❖ Unrestricted Hartree-Fock Method (URHF)

Using two entirely different sets of orbitals for the α and β electrons is one method of producing Hartree-Fock wavefunctions from molecules with unpaired electrons. The unrestricted Hartree-Fock wave function (UHF) is the term for this. This implies that coupled electrons will have a different spatial distribution [78]. Two sets of spatial orbitals, one with up-spin (α) electrons and the other with spin-down (β) electrons, are used in this method.

2.7 Density Functional Theory (DFT) Method

Thomas and Fermi developed an approximated version of DFT in 1927, shortly after the development of quantum mechanics [79]. Density functional theory replaces the many-body electronic wave function with the electronic density as the fundamental in an effort to address both the inaccuracy of HF and the high computational demands of post-HF methods. While electron correlation is included indirectly from the beginning, density is a function of only three variables and is a simpler quantity to deal with both conceptually and practically. The wave function of N electrons system depends on $3N$ variables (three spatial variables for each of the N electrons) [80, 81]. DFT can be used to calculate a wide range of molecular properties, facilitating close collaboration between theory and experiment. It can also provide significant hints about the geometric, electronic, and spectroscopic

properties of the systems. The fundamental tenet of density functional theory is that a system's density can be used to determine its energy:

$$(2\text{-}16) \quad E = E(\rho)$$

 Due to the DFT's superb performance could be attributed to these approximation functionals, DFT applications have skyrocketed across numerous chemical domains. In DFT, the only thing to look for is the three-dimensional density given an exchange correlation functional in a given form [82]. The following equation can be used to determine a system's ground-state energy:

$$E_{DFT}[\rho] = T[\rho] + J[\rho] + E_{ne}[\rho] + E_{XC}[\rho] \qquad (2\text{-}17)$$

A non-interacting system's kinetic energy is denoted by $T[\rho]$. The electron-electron repulsion energy is $J[\rho]$, while the external potential is $E_{ne}[\rho]$. Finally, the exchange-correlation energy functional is $E_{XC}[\rho]$.

Summing the exchange function E_X and the correlation function E_C yields the exchange and correlation function $E_{XC}[\rho]$.

$$E_{XC} = E_X + E_C \qquad (2\text{-}18)$$

DFT was later developed by Kohn and Sham in 1964–1965 to get around the challenges of "first principles" techniques. Hohenberg and Kohn's two theorems served as the foundation for this work [83, 84].

The total number of electrons is obtained by taking the integral of the electron density, as shown in the following equation:

$$\int \rho(\vec{r})dr = N \qquad (2\text{-}19)$$

The relationship between $\rho(r)$ and the many-electron wavefunction Ψe can be expressed as follows:

$$\rho(\vec{r}) = N \int \ldots \int |\Psi(\vec{r}_1\vec{r}_2, \ldots, \vec{r}_N)|^2 d\vec{r}_1 d\vec{r}_2 \ldots d\vec{r}_N \qquad (2\text{-}20)$$

The probability of discovering any of the N electrons inside the volume element dr_n is represented by $\rho(\vec{r})$ [85].

2.7.1 Hohenberg- Kohn (HK) Theorems

As Hohenberg and Kohn proved in 1964, the ground state of a many-electron system can be found from the ground state electron density $\rho(r)$. The two theorems by Hohenberg and Kohn's are:

❖ First Theorem

According to the first HK theorem, an electron density that depends only on three spatial variables can uniquely define the ground-state features of a many-electron system. It offers the basis for applying the electron density functional to reduce the many-body problem of N electrons with $3N$ spatial coordinates to three spatial dimensions [86]. They proposed their first theorem, which is as follows: Imagine an arbitrary number of electrons contained in a sizable box and imagine them transferring via Coulomb mutual repulsion and the external potential [87, 88]. The Hamiltonian has the following form:

$$H = T + V + U \tag{2-21}$$

where T represents the N-electron kinetic energy, V represents the N-electron potential energy from the external field, and U represents the electron-electron dissonance [83, 89].

❖ Second Theorem

It is possible to define a universal functional $E[\rho]$ for the energy in terms of density. The global minimum value of this functional represents the accurate ground state. In order to determine the ground-state energy for the external potential, the functional could therefore be minimized by changing the density [90]. They demonstrate how the minimum of the

energy functional according to the electron density can be used to calculate the ground state energy [89].

$$E\left(\rho_0\right) = Min\ E\left(\rho\right) \tag{2-22}$$

2.7.2 Kohn-Sham (KS) Method

The Kohn–Sham density functional theory (KS-DFT) is a very useful method for figuring out a material's electronic structure. Exchange-correlation (XC) hybrid and generalized gradient approximations can be utilized to achieve meaningful accuracy [91]. Formally, KS-DFT is exact because it guarantees the exact ground-state density ρ(r) and energy given the exact exchange-correlation (XC) energy functional through a numerically exact solution of the self-consistent KS-DFT equations. It also provides a time-independent external potential v(r) for any system of N electrons. The true ground-state electron density of an N-electron system can be constructed from the N one-electron orbitals of the lowest energy of a specific independent electron system, according to (KH) theory [87]. The following equation provides a summary of this:

$$\hat{H}_{ks}\,\psi_i = E\psi \tag{2-23}$$

Density-functional theory-based techniques currently predominate in condensed matter and most quantum chemistry first-principles calculations [92].

Therefore :

$$\left[\frac{-\hbar^2}{2m}\nabla^2 + V_{ion}(\vec{r}) + V_H(\vec{r}) + V_{Xc}(\vec{r})\right]\psi_i(\vec{r}) = \varepsilon_i\psi_i(\vec{r}) \tag{2-24}$$

The particle's total energy is represented by ε_i. The electron wavefunction is $\psi_i(\vec{r})$. Which represents the de Broglie wave connected to the particle mathematically. However, the system's effective potential can be determined by:

$$V_{eff} = V_H + V_{XC} + V_{ext} \tag{2-25}$$

While (V_{ext}) represents the nuclei potential, $V_H(\vec{r})$ represents the Hartree potential, which is given by:

$$V_H(\vec{r}) = \int \frac{\rho(\vec{r}_1)\rho(\vec{r}_2)}{|\vec{r}_1 - \vec{r}_2|} d\vec{r}_1 d\vec{r}_2 \tag{2-26}$$

Where V_{XC} is the exchange and correlation potentials, which can be expressed as:

$$V_{XC} = V_C + V_X \tag{2-27}$$

So, the Kohn-Sham equation can be set as:

$$\hat{H}\psi_i(\vec{r}) = \left[\frac{-\hbar^2}{2m}\nabla^2 + V_{eff}(\vec{r})\right]\psi_i(\vec{r}) = \varepsilon_i\psi_i(\vec{r}) \tag{2-28}$$

So far, the energy exchange and correlation cannot be overcome in a systematic way. But it wasn't until the development of estimated ion methods in 1990, which greatly aided in modeling the exchange-correlation relationship, that DFT showed useful in quantum chemistry. There for, DFT is a top instrument for determining electronic structure in many different domains [93].

2.8 The Exchange-Correlation Functionals

According to Hohenberg, Kohn, and Sham, the basis of DFT is the observation that a uniform electron density can only precisely calculate the sum of its exchange and correlation energies [94]. The ground state properties can be well described by DFT, which is based on the so-called exchange-correlation functional. According to the Pauli principle, exchange interaction characterizes the quantum mechanical effect between identical particles in a system. The Coulomb interactions that occur between electrons in a system are related to correlation energy [95]. The energy of correlation and exchange is proposed in several ways. The

first successful approximation was the Local Density Approximation (LDA), which is a local functional because it depends only on density. The Generalized Gradient Approximation (GGA), which was semi-local due to the inclusion of the density derivative, was the next step. The two most commonly used approximations to the exchange and correlation energies in density functional theory are LDA and GGA. In addition to LDA and GGA, multiple other operations, exist [96].

2.8.1 Local Density Approximation (LDA)

The local density approximation (LDA) is the most widely used approximation in physics. For many years, the LDA has been used in calculations of band structures and total energies in condensed matter physics. The exchange-correlation energy can be given by:

$$E_{xc}^{LDA}\big(\rho(\vec{r})\big) = \int \big(\rho(\vec{r})\big)\varepsilon_{xc}\rho(\vec{r})d^3\vec{r} \tag{2-29}$$

XC represent the energy per particle in an electron gas with a uniform density of $\rho(\vec{r})$, which is given by ε_{xc}. While highly accurate data based on quantum Monte-Carlo simulations are available for the correlation part of the LDA XC functional, the exchange part of the functional can be determined precisely.

Several physical properties can be computed with a high degree of accuracy using LDA, and many ground state properties are well-described in the LDA, which is the primary benefit of LDA-DFT over schemes like Hartree Fock [97].

2.8.2 Generalized Gradient Approximation (GGA)

The generalized gradient approximation (GGA), a kind of straightforward extension of LDA, is more frequently applied in quantum chemistry [98]. It enhances LDA by adding gradient terms to account for

density change near r. Unlike the LDA, the GGA formulation has multiple kinds instead of a single definition. The GGA is extended to magnetically polarized systems in a manner akin to the LDA. The GGA is not a consistently better solution to the local approximation; however, it does perform better in some areas where the LDA does not. The undervaluation of the exchange energy and the enhancement of the correlation energy in the LDA form the foundation of the GGA [99].

$$E_{XC}^{GGA}[\rho] = \int \rho(\vec{r})\epsilon_{XC}^{GGA}(\rho(r) \, \nabla\rho(\vec{r}))d^3r \qquad (2\text{-}30)$$

It has been discovered that GGA is especially effective at calculating the material's structural properties for XC energy. It has a high enough accuracy level to help with forecasting and even data interpretation [97].

2.9.1 Hybrid Functionals

It has been demonstrated that hybrid functionals that incorporate a certain level of Hartree-Fock (HF) exchange into a local or semi-local density functional can address several shortcomings. It is recognized that HF/DFT hybrid functionals, or exchange-correlation functionals, offer a better explanation of the thermochemistry of molecular systems [100]. The most commonly used hybrid functional, for instance, is the B3LYP [101, 102]. It combines the Beckes gradient-corrected exchange functional with the Lee, Yang, and Parrs gradient-corrected correlation functional, (Becke, three-parameters, Lee-Yang-Parr) [103, 104]:

$$E_{xc}^{B3LYP} = E_{xc}^{LDA} + a_0(E_x^{HF} - E_x^{LDA}) + a_x(E_x^{GGA} - E_x^{LDA})$$
$$+a_c(E_c^{GGA} - E_c^{LDA})$$

$$(2\text{-}31)$$

Where $a_0, a_x,$ and a_c are three empirical parameters, the following was the value of these found $[a_0 = 0.20, a_x = 0.72,$ and $a_c = 0.81]$.

29.2 Programs Used in this Work

2.9.2.1 Gaussian 09W

Gaussian starts in 1970 with the fundamental ideas of quantum mechanics and goes on to predict many molecular properties that are derived from these basic computation types, including energies, molecule structures, and vibrational frequencies of molecular systems. It can be applied to study molecules and reactions in a range of situations, including compounds and stable species that are hard or impossible to find through experimentation, like transition structures and short-lived intermediates [105]. The Roothaan-Hull equation is the basis for the Gaussian program, which calculates the maximum number of periodic table elements. The accuracy of the calculations in this program depends on the number of wavefunctions or basis sets used; the higher the number, the more significant the result [106]. For all computational calculations, the Gaussian 09 software [107] with the GaussView 06 [108] graphical user interface was utilized.

2.9.2.2 GaussView Program

In addition to offering intermediate and final computation results, the GaussView program is a graphical redactor for the Gaussian program that makes setting up an input file and structure for the Gaussian program relatively easy. The routines in GaussView 06 can be utilized in addition to the main program. This makes it possible to graphically represent molecular structures [109].

2.10 Basis Sets

The goal of a basis set is to give the best possible representation of the electron density, or unknown chemical orbitals, at the lowest possible computational cost [110]. Another view for the basis set is a group of

mathematical functions that is used in theoretical computation and modeling to build a quantum mechanical wavefunction of a system [111]. Choosing the right basis set is essential to obtaining useful outcomes from a quantum chemical calculation. A quantum chemical problem can be solved with any full basis set [112]. These functions are frequently based on atomic nuclei, and the electron distribution around each atom is represented by a variety of basis functions. The electron distribution throughout the molecule is obtained by integrating the atomic basis functions. Atomic orbital wavefunctions can be approximated well by a specific kind of basis function called a Slater-type orbital (STO). However, it is challenging to evaluate most basis sets approximate the STOs using different combinations of Gaussian-type orbitals (GTOs). In a minimal basis set, all the electrons in each atom can be described by the minimal number of basis functions [113].

2.10.1 Minimal Basis Sets

The minimal number of atomic orbitals needed to contain every electron in a particular atom makes up the minimal basis set. The Slater type and the Cartesian Gaussian type are the two types of function representations of minimal basis sets of atomic orbitals that are most frequently used [72]. The notation STO-3G indicates that the basis set approximates the form of the STO orbital, using a single contraction of three Gaussian functions [114]. Despite being less computationally expensive than their larger counterparts, minimal basis sets frequently yield much less accurate results [113].

2.10.2 Split Valence Basis Sets

In most molecular interactions, the valence electrons play a major role in the bonding process. This leads to the representation of valence orbitals

by multiple basis functions, each of which is a fixed linear combination of primal Gaussian functions. The term "valence basis sets" refers to valence double, triple, quadruple-zeta, and other basis sets that have multiple basis functions matching each valence atomic orbital (zeta ζ was commonly used to denote the exponent of a STO basis function) [115]. The majority of basis sets including split-valence sets have basis functions composed of several Gaussian functions rather than just one. The contraction scheme is defined by the ubiquitous split-valence 6-31G basis set. The boundary between the valence (on the right) and the core (on the left) is indicated by the dash. According to this scenario, each core basis function is made up of six Gaussian functions. Two fundamental functions that make up the valence space are known as "inner" and "outer" functions. A group of functions known as polarization functions can be added to basis sets in order to increase their completeness [116]. The available Pople basis sets are as follows: 3-21G, 4-31G, 6-21G, 4-22G, 6-311G, and 7-41G [78].

2.10.3 Polarized Basis Sets

Can append one or two asterisks to the Pople basis set notation, such as 6-31G* or 6-31G**. A single asterisk indicates that a set of d primitives has been added to an atom that is not hydrogen. Two asterisks indicate that hydrogen has also been supplemented with a set of P primitives. Because they enable the wavefunction to change shape more quickly, these are referred to as polarization functions. The variational total energy is decreased by adding polarization functions in a manner similar to that of adding another contraction. However, this energy change has little effect on relative energies because it is nearly totally systematic. Polarization functions are widely used because they

frequently produce more precise calculated geometries and vibrational frequencies [78].

2.10.4 Diffuse Basis Sets

A more comprehensive form of s and p-type functions are diffuse functions. They allow orbitals to travel through more space. Diffuse functions found in basis sets are useful for systems like anions, molecules with lone pairs, effective negative charge systems, excited state systems, low ionization potential systems, and so on, where the electrons are comparatively far from the nucleus [116].

The symbols below are commonly used to indicate the spread function when using it :

+ for heavy atoms (apart from hydrogen).

++ for hydrogen and heavy atoms.

2.11 Roothaan – Hall Equations and the Linear Combination of Atomic Orbitals (LCAO)

The HF approach produces a complicated system of nearly unsolvable integro-differential equations that are easily resolved problems. A non-orthonormal basis set, which could be Slater-type or Gaussian, is represented by the Roothaan equations for the Hartree-Fock equation. The linear combination of atomic orbitals (LCAOs) and the variational principle are applied to the HF equation to derive the Roothaan-Hall equations. In theory, the Hartree-Fock problem can be resolved using any standard method for integrating differential equations [88].

2.11.1 Slater-Type Orbitals (STOs)

Atomic orbitals used in the linear combination of atomic orbitals and molecular orbital technique are known as Slater-type functions. STO was

created by Zener and Slater for multi-electron atoms [117, 118], and the method is largely dependent on the basis functions that are employed for the reliability of the electronic distribution that they provide [119]. The definition of the slater-type function is [120]:

$$\Psi_{nlm}^{STO}(r, \theta, \phi) = R_{nl}(\vec{r})Y_{lm}(\theta, \Phi) \tag{2-32}$$

Where m is the magnetic quantum number, n is the principal quantum number, and l is the orbital quantum number. The spherical harmonic $Y_{lm}(\theta, \Phi)$ and the radial part of the atomic functions for STOs are represented by $R_{nl}(\vec{r})$ as follows:

$$R_{nl}(r) = N_n r^{n-1} exp(-\zeta r) \tag{2-33}$$

 And:

$$Y_{lm}(\theta, \phi) = \theta_l(\theta)\phi_m(\phi) \tag{2-34}$$

 Where ζ, is the orbital exponent, which is given by:

$$\zeta = \frac{z-s}{n^*} \tag{2-35}$$

Also, N is the normalization constant.

 Where n^* is the active main quantum number, s is a protection parameter, and z is the number of atoms. An empirical value for the shielding parameter, s, is provided based on n and l.

2.11.2 Gaussian-Type Orbitals (GTOs)

Gaussian-type orbitals (GTOs) are widely used in standard quantum chemistry packages to characterize the electronic structure of nonlinear molecules. Slater-type orbitals (STOs) are almost exclusively used in the computation of atoms and linear molecules because they can efficiently handle the multicenter integrals that arise in nonlinear calculations, despite having the appropriate "cusp" near nuclei and correct asymptotic

behavior. On the other hand, when GTOs are employed, such integrals can frequently be evaluated in closed form. The dominance of GTOs in molecular electronic structure calculations can be attributed to this fundamental advantage [121].

$$\Psi_{nlm}^{GTO}(r,\theta,\phi) = R_{nl}(r)Y_{lm}(\theta,\Phi) \qquad (2\text{-}36)$$

$$R_{nl}(r) = N_n r^{n-1} exp(-\zeta r^2) \qquad (2\text{-}37)$$

Instead of depending $exp(-\zeta r)$ the radial type in GTO depends on $exp(-\zeta r^2)$. In contrast to STOs, which can only be solved numerically, this allows the electron-electron repulsion integrals to be solved analytically. The primary drawback of GTOs is that they lack the appropriate "cusp" at the nucleus, and their exponent rapidly approaches zero as r increases, as shown in Figure (2.1) the comparison between STO and GTO functions [122]:
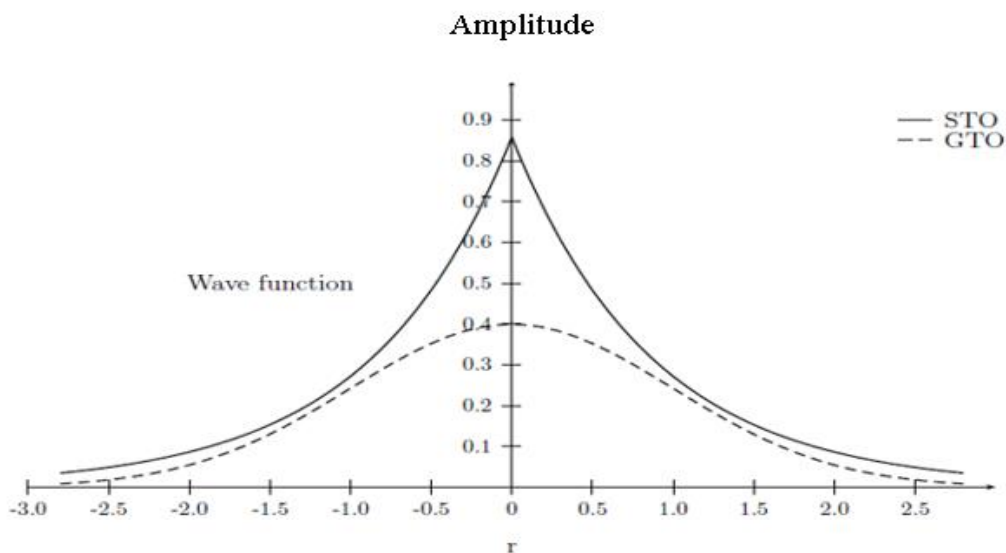
Figure 2.1: A comparison between the STO and GTO functions.

2.12 Atomic Charge

The application of quantum computations to the molecular system was greatly aided by efficient atomic computations. These calculations deal with the effects of atomic charges on dipole moment, polarizability of molecules, and other properties of molecules [123-125].

Mulliken is considered the most economical and rapid way to figure out charges. But at best, this method yields only qualitative results. It is clear what the reason is. There is absolutely no polarization, and the participating atoms' canonical orbits will be divided equally among them. They also depend on the basis set, so expanding the basis set makes the description worse [126].

The Lewis-like molecular bonding pattern of electrons is represented by natural bond orbitals (NBO), which are a collection of localized few-center orbitals that are optimally condensed and orthonormal. The information about interactions in both filled and virtual orbital spaces that the NBO method provides could expand the analysis of intra- and intermolecular interactions (the interaction between electron donors and electron acceptors). This is why the NBO method is useful. A stabilizing donor-acceptor interaction is characterized by the delocalization of electron density between occupied Lewis-type (bond or lone pair) NBO orbitals and formally unoccupied (anti-bond) non-Lewis NBO orbitals [127].

2.13 Non Linear Optical (NLO) Properties

The nonlinear optical characteristics of polymeric materials have garnered significant interest due to their possible uses in integrated optics, electro-optic modulation for optical telecommunication and optical interconnects, and frequency doubling for data storage [128]. To

determine the relationship between molecular structure and non-linear optic characteristics (NLO), it is important to investigate the dipole moment (μ), polarizability (α), first-order hyperpolarizability (β), and optical susceptibility of the PI molecule.

2.13.1 Dipole Moment (μ)

It is expressed as a vector in three dimensions and measures the asymmetry (polarity force) in the molecular charge distribution [129]. Dipole moments (μ) is related to the stability of molecules, it is a crucial topic in polar environments [126]. The dipole moment of a molecule is the quantity that is most frequently used to explain polarity. It is a reliable sign of the asymmetry of a molecule [130]. The distance between the two linked atoms and the charge of the atoms determine it. The entire molecule's absolute polarity is represented by the total dipole moment. The total molecular dipole moment for a given molecule can be found using the vector sum of the individual dipole moments [131].

The equation below can be used to evaluate the total dipole moment in terms of its components [132].

$$\mu_{tot} = \left(\mu_x{}^2 + \mu_y{}^2 + \mu_z{}^2\right)^{1/2} \tag{2-38}$$

2.13.2 Polarizability, First-Order Hyperpolarizability, and Optical Susceptibility

A molecule's power can react to an electric field and generate an electric dipole moment is known as its polarizability. Either a permanent or an electric field-induced electric dipole moment can exist [133].

The following formulas can be used to determine the anisotropy of the polarizability ($\Delta\alpha$) and the mean polarizability ($\bar{\alpha}$) [134].

$$\bar{\alpha} = \frac{1}{3}(\alpha_{xx} + \alpha_{yy} + \alpha_{zz}) \tag{2-39}$$

$$\Delta\alpha = \frac{1}{\sqrt{2}}\left[\left(\alpha_{xx} - \alpha_{yy}\right)^2 + \left(\alpha_{yy} - \alpha_{zz}\right)^2 + (\alpha_{zz} - \alpha_{xx})^2 + 6\alpha_{xz}^2 + \right.$$

$$\left. 6\alpha_{xy}^2 + 6\alpha_{yz}^2 \right]^{\frac{1}{2}} \tag{2-40}$$

A third-rank tensor, the first-order hyperpolarizability, can be explained by a 3×3×3 matrix. Because of the Klein symmetry, the 27 components of a 3D matrix can be reduced to 10 components. It is possible to compute the components of the initial hyperpolarizability by utilizing the following formula, utilizing the components x, y, and z [135]:

$$\langle\beta\rangle = \left[\left(\beta_{xxx} + \beta_{xyy} + \beta_{xzz}\right)^2 + \left(\beta_{yyy} + \beta_{yzz} + \beta_{yxx}\right)^2 + \left(\beta_{zzz} + \beta_{zxx} + \beta_{zyy}\right)^2\right]^{\frac{1}{2}} \tag{2-41}$$

The most fundamental parameters that describe light-matter interactions and determine optical applications in any material is the complex optical susceptibility [136]. The average value of the susceptibility χ can be given by [51] :

$$\chi = \frac{N\alpha'}{1 - \frac{4\pi N\alpha'}{3}} \tag{2-42}$$

Where α': Polarizability volume, which can be given by:

$$\alpha' = \alpha/4\pi\varepsilon_O \tag{2-43}$$

N: Molecular number density, which can be provided by:

$$N = \rho\, N_A/M_W \tag{2-44}$$

M_W: Molar mass, N_A: Avogadro's number and χ: Susceptibility.

2.14 Vibrational Frequencies

Vibrational modes of infrared-active molecules can be identified by their frequency, which corresponds to a particular stretch or bend. These modes can vibrate in a variety of ways, depending on whether they are

bending or stretching. Bending modes modify the bond angle while keeping the bond length constant, whereas stretching modes change the bond length while maintaining the bond angles. Along with a variety of bending modes like scissoring, wagging, rocking, and twisting, there are two types of stretching modes: symmetric and asymmetric stretching, see Figure (2.2).

Figure 2.2: Various vibrational modes [137].

2.15 Infrared Spectroscopy (IR)

The general term for the visualization of functional groups found in a sample is infrared spectroscopy. The procedure involves determining which infrared wavelengths are absorbed by the various kinds of bonds. The necessary wavelengths and frequencies for inducing bond vibration in molecules are found in infrared radiation. For bonds to absorb infrared light, they need to show a time-dependent dipole [138].

Many scientific fields use vibrational spectroscopy as a basic technique for chemical analysis, and it is well known that infrared (IR) absorption spectroscopy offers supplementary knowledge about molecular vibrations. For the purpose of identifying a molecule's functional groups, IR absorption spectroscopy is frequently used. This technique is effective for polar bonds like O-H or N-H. Every vibration can be caused by two atoms moving together or by a group of atoms moving together [139].

Infrared radiation has a lower frequency in the visible electromagnetic spectrum than red light. Between the visible and microwave spectra is the infrared spectrum. A large portion of the electromagnetic spectrum is covered by it. Compared to visible radiation, infrared radiation has less energy. The infrared region can be classified into three sections: firstly, the near Infrared (NIR). Secondly, the mid infrared region (MIR). Thirdly, the far infrared region (FIR) [140]. The mid-region, which is between (4000 and 200) cm^{-1}, and the far-region, which is between (200 and 10) cm^{-1}, comprise the near-infrared region (13000-4000) cm^{-1}. When energy is absorbed, the N-atom system oscillates with three degrees of freedom, and ring molecules have three degrees of freedom for vibration $(3N-6)$ [141].

A molecule's spatial distribution, or whether it is linear or non-linear, determines how many vibrational transitions it has in addition to the number of atoms that make up the molecule .

❖ In the case of linear molecules, there are $3N - 5$ vibrational modes.

❖ In the case of nonlinear molecules, there are $3N - 6$ vibrational modes .

Where N is the molecule's atomic count. And that's how the vibrational modes are represented [142].

2.16 UV-Vis Absorption Spectroscopy

The method of measuring the wavelength and intensity of ultraviolet and visible light absorbed by a sample is called UV-vis spectroscopy. UV spectroscopy is typically used to examine molecules in solution and inorganic compounds. Photons of ultraviolet and visible light possess enough energy to accelerate outer electrons and trigger higher energy states. Chemical bonds are created by overlapping atomic orbitals, and these bonds can lead to low-energy, high-energy, or non-bonding molecular orbitals. Energy absorption is typically linked to electron transitions from bonding to anti-bonding orbitals [143].

Chapter Three

Chapter Three

Results and Discussion

3.1 Introduction

In this chapter present will to the findings from the DFT approach with the hybrid function B3LYP and discuss the results for polyimide. This was done in two stages. The structure properties, such as the potential energy surface, the lowest energy required to obtain the optimal structure, the bond lengths, bond angles, dihedral angles, and charge distribution, are presented in the first stage. While, the second stage dealt with the optical properties, which included first-order Hyperpolarizability, Polarizability, susceptibility, dipole moment and spectral properties such as Infrared spectroscopy, and UV absorption spectroscopy. In all stages, Gaussian 09 has performed all calculations. GaussView 06 is used as an additional tool to discover the optimization geometries.

3.2 Simulating the Monomer of PI

Figure 3.1 shows the simulation of the monomer PI in its natural pattern. It has 22 carbon atoms, 12 hydrogen atoms, 5 oxygen atoms, and 2 nitrogen atoms. For the purpose of obtaining its structural and optical characteristics, it was constructed using the GaussView 06 software and optimized using the Gaussian 09 program. These properties were computed using the density functional theory DFT/ B3LYP and with the basis set 6-311G (d, p).
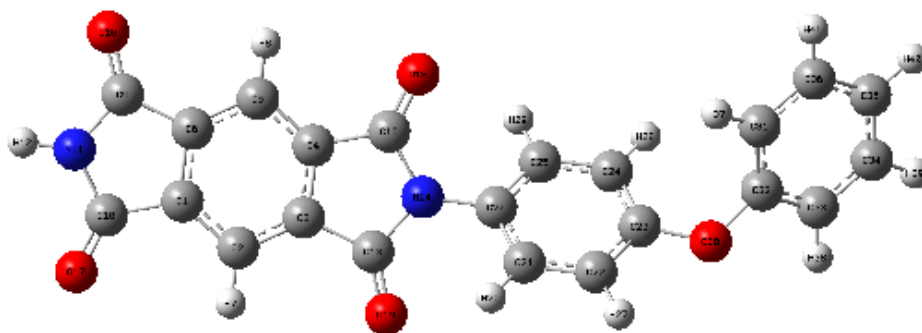
Figure 3.1: The PI monomer drawing by GaussView06.

3.3 Structural Properties

3.3.1 Potential Energy Surface (PES) Scan

The potential energy surface is a theoretical tool for helping with the investigation of molecular geometry and chemical reaction kinetics after the synthesis of the monomer. The potential energy surface clarify the idea that each atom's and molecule's internal and external geometries in a chemical reaction have a distinct potential energy. The monomer's partial optimization was discovered using a scan.

Using the semi-empirical method PM6, the scan has been carried out for the two dihedral angles SC1=C15-N14-C20-O25 and SC2=C23-C24-O30-C32 (see Figure 3.2). The dihedral angles SC1 and SC2 are modified in this method from 0°–360° by 10 for each phase. The other geometries are left to remain relaxed while the scan calculations adjust the dihedral angles. The scan grid is then created, as shown in Figure 3.2. It contains 1369 molecules with various energies and several global maximums and minimums.The lowest-energy molecule should be identified in order to determine which of the 1369 molecules is the most stable. Minimum energies are shown in the scan grid at dihedral angles SC1 and SC2. The optimization will only be partial due to the low precision of the PES scanning techniques and the semi-empirical PM6 [144].

Furthermore, conformer curves can only yield approximate findings for locating stable energy points. They are a valuable tool for identifying the appropriate conformer for computations requiring a greater level of precision. As in Figure 3.3, (A) is a maximum energy of (-0.13265 Hartree), and which represent molecule 513, which has SC1 = 88 and SC2 = 358, is considered the un stable one with the maximum energy. Also, as Figure 3.3, (B) is a minimal energy of (-0.13581 Hartree), and which represent molecule 477, has SC1 = 208 and SC2 = 148, is considered the stable one with the minimum energy.

.
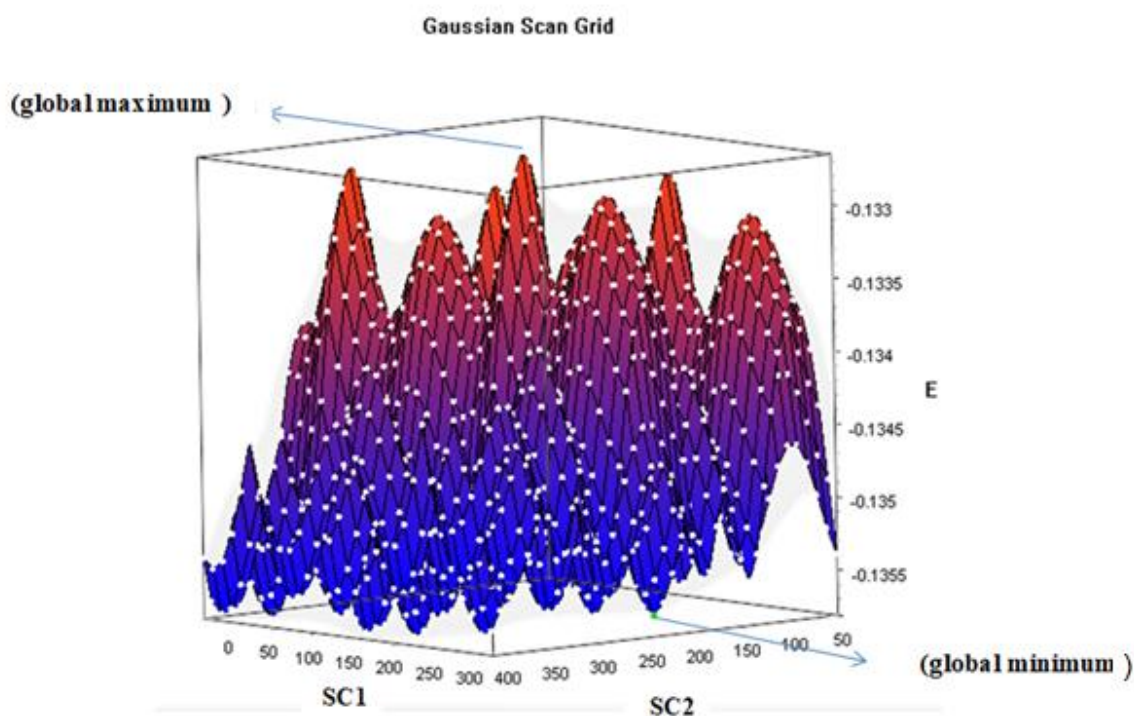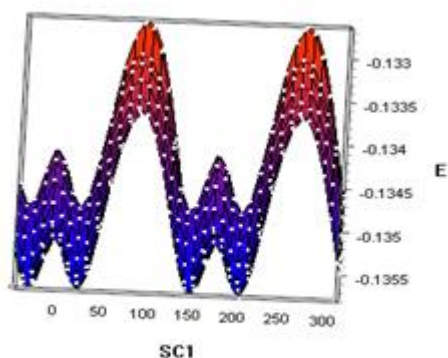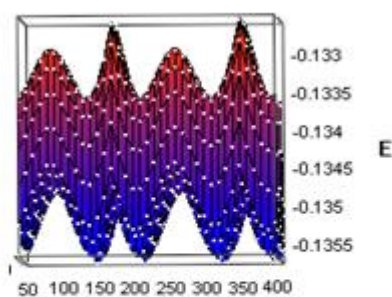
Figure 3.2: (A) represent a 3D surface contains 1369 molecules with various energies and several global maximums and minimums using the semi-empirical method (PM6). The global maximum energy was found at molecule 513 which has dihedral angles SC1=88, SC2=358, and E= - 0.13265 Hartree, whereas the global minimum energy was found at molecule 477 with dihedral angles SC1=208, SC2=148, and E= - 0.13581 Hartree. B and C: represent a 2D Gaussian scan grid of a potential energy surface for the PI molecule with dihedral angles.
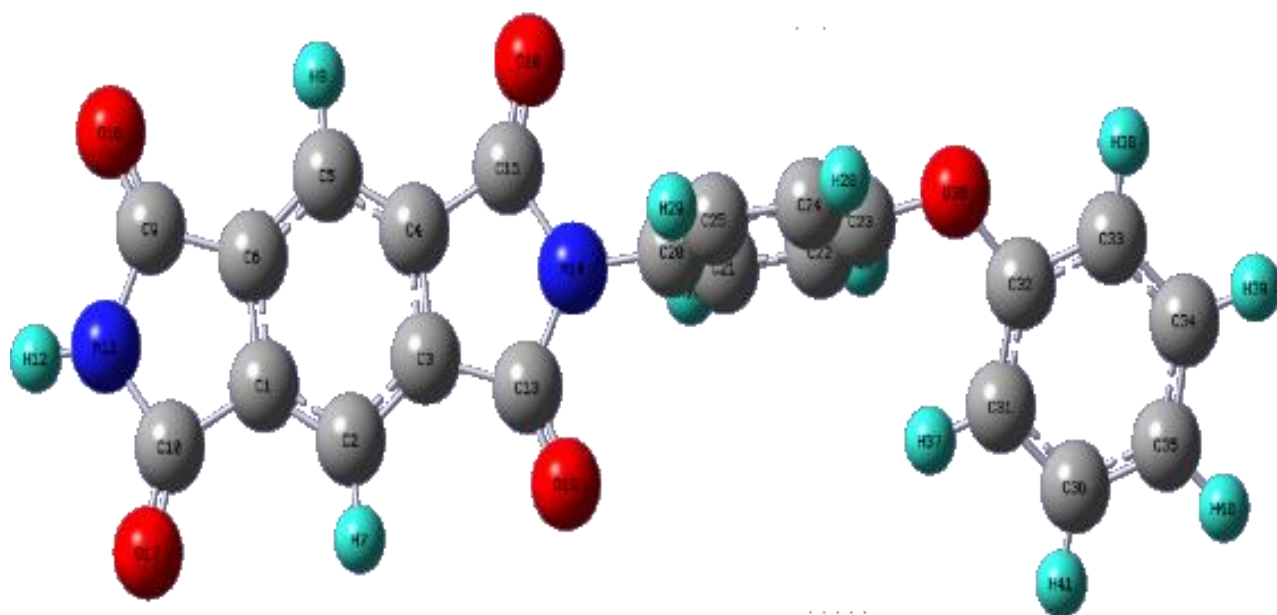
(A) Molecule 513
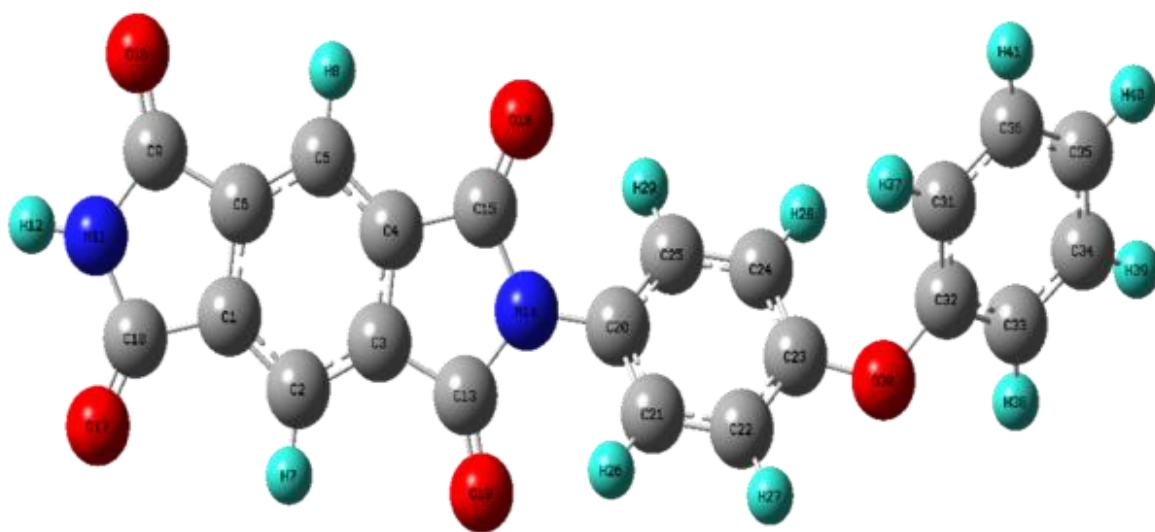
(B) Molecule 477

Figure 3.3: (A) Molecule 513 with SC1=88, SC2=358, and E = -0.13265 Hartree
(maximum energy). (B) Molecule 477 with SC1 = 208, SC2 = 148 and
E = -0.13581 Hartree (minimum energy).

3.3.2 Full Optimization of PI

The PI monomer is completely optimized using the DFT/ B3LYP with a 6-311G (d, p) basis set after the potential energy surface. The calculations are converged to optimized geometries that correspond to true energy minima. The dihedral angles SC1 and SC2 were somewhat changed by the application of the DFT, going from 208.4° and 148.6° to 220° and 214°. The accuracy of the dihedral angles obtained with DFT has been verified by means of the potential energy curve. The total electronic energy decreases with the dihedral angles up to around 220º, as Figure 3.4. At 214 degrees, Figure 3.5 exhibits the same behavior with the lowest energy. These findings verify the accuracy of the dihedral angles that determine the energy of the molecule.

The reduction of energy is improved by the absence of imaginary frequencies and the convergence of the four criteria (RMS force, maximum force, RMS displacement and maximum displacement). So the resulting molecule was discovered to be optimized and converged. Geometries having a -1331.578 Hartree correspond to the minimum energy.
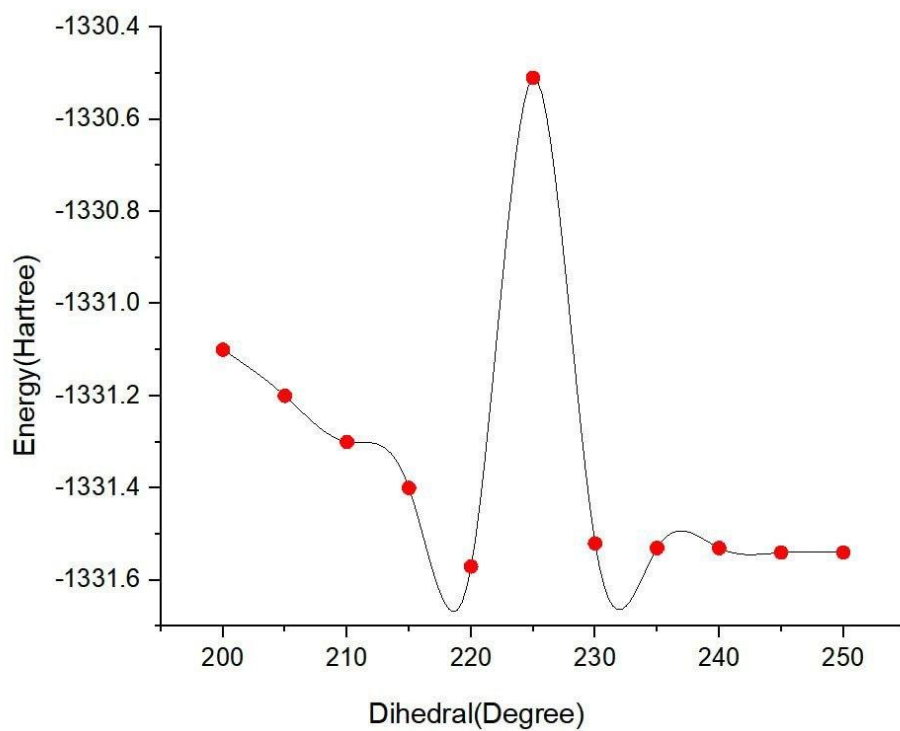
Figure 3.4: The potential energy curve for the angle SC1.
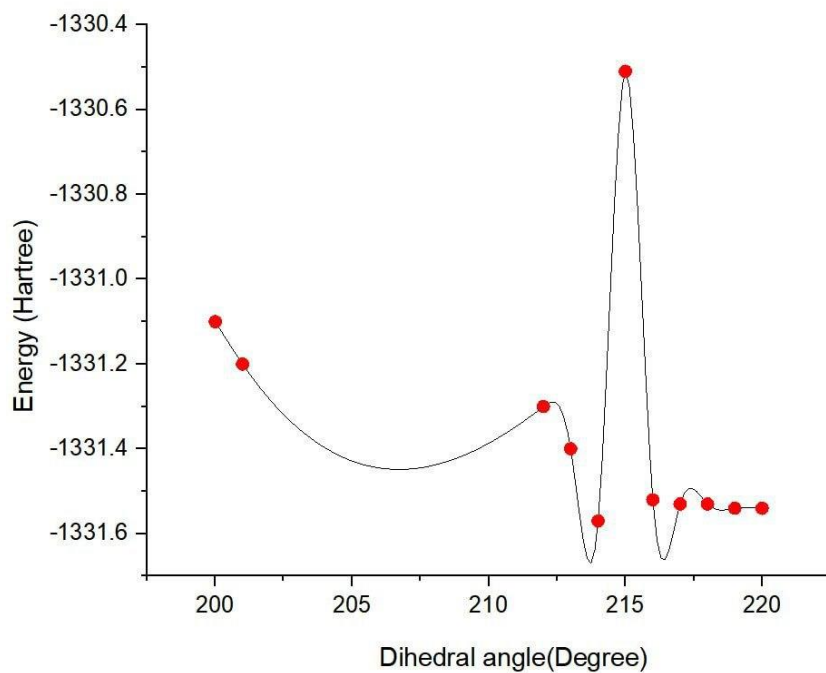
Figure 3.5: The potential energy curve for the angle SC2.
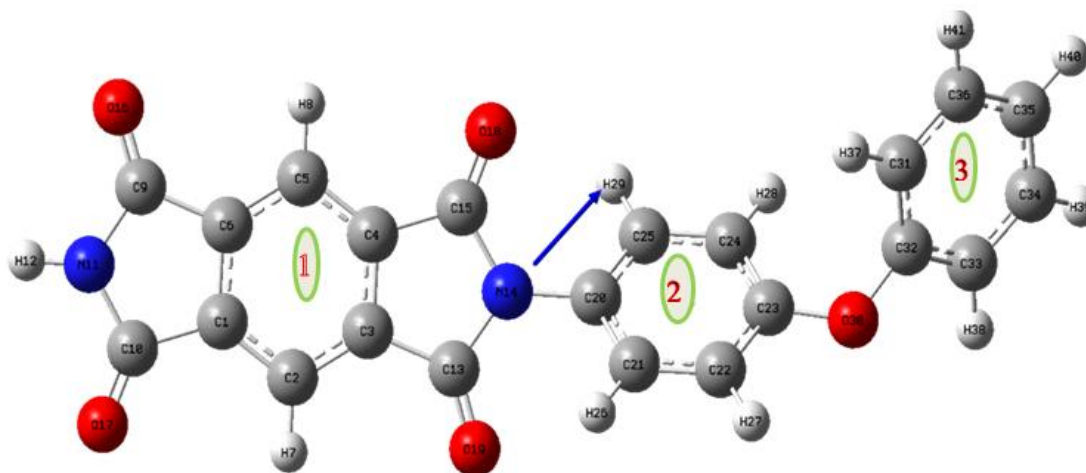
Figure 3.6: The structure of PI after a fully optimized geometric with a dipole moment vector.

3.3.3 Bond Lengths

Compared to other molecular parameters, bond lengths have likely been used to classify chemical bonds [145]. The outcomes match the experimental values in a dependable method [39, 44], the properties studied show that the C-C, C-N, and C-H ring bonds are typical of covalent interactions. In Table 3.1, the average of the first benzene ring bond length was determined to be 1.391Å, which closely matched the experimental value of 1.396Å. Similarly, the average of the second ring and the third ring bond lengths was found, respectively, to be 1.391Å and 1.393Å, which is closely related to the experimental values of 1.380Å and 1.387Å, respectively. In addition, the average values of the bond lengths for the total rings are calculated to be 1.392 Å theoretically and 1.897 Å experimentally [35].

Figure 3.6 shows the benzene rings (1, 2, and 3). The C and N atoms in the PI have bond lengths of 1.41 in the Angstrom unit. For comparison, the bond C23-O30 values are determined to be 1.374Å, which is close to the experimental value of 1.390Å. Theoretically, the average bond lengths for aromatic hydrogen atoms are determined to be 1.086 Å.

It is important to note that the lengths of single C-C atom bonds outside of the ring, such as C1-C10, C3-C13, C4-C15, and C6-C9, are greater than those of aromatic bonds. This phenomenon happens because of the p-electrons and benzene ring resonance. One p-electron is present in each carbon atom, and these electrons overlap to form a system of orbitals that spread out throughout the carbon atoms. Three molecular orbitals will delocalize the six electrons because they are no longer held between just two carbon atoms. This delocalization gives the benzene ring more stability. As a result, the bond lengths between carbon atoms will be the same as or shorter than those found outside of the ring.

Bond length decreases as the number of electrons involved in bond formation increases because bond length is proportional to bond order. Additionally, the bond strength and bond dissociation energy are inversely correlated with the bond length or distance.

It is also notable that the C9=O16 double bond is shorter than the C9-N11 and C23-O30 bonds because its electrons occupy more space due to its greater electron density than those of a single bond (the force of attraction between atoms is more significant in the double bond, causing the atoms to be pulled). The C13=O19 and C15=O18 bonds exhibit exactly identical circumstances. The bond lengths of the C23-O30 are shorter than those of the C23-C24 due to the strong electronegativity of oxygen atoms, which causes the electron density to move closer to the nucleus.

 In conclusion, there is good agreement between the experimental and DFT results for bond lengths. Table 3.1 shows the polyimide molecule's bond length using DFT/B3LYP with 6-311G (d,p).

Table 3.1: Bond lengths of PI in Angstrom unit.

Bond	Bond Length	Experimental [39, 44]	Bond	Bond Length	Experimental [39, 44]
C1-C6	1.389	1.385	C6-C9	1.498	1.490
C1-C2	1.389	1.397	C9-N11	1.400	1.40
C1-C10	1.498	1.490	C9=O16	1.204	1.187
C2-C3	1.389	1.390	C10-N11	1.400	1.41
C3-C4	1.394	1.396[44]	C10=O1	1.204	1.187
C3-C13	1.493	1.490	C13-N14	1.414	1.40
C4-C5	1.389	1.413[44]	N14-C15	1.414	1.40[44]
C4-C15	1.493	1.480[44]	C15=O1	1.204	1.22[44]
C5-C6	1.389	1.397	C13=O1	1.204	1.187
N14-C20	1.429	1.428[44]	C24-C25	1.390	1.390
C20-C21	1.397	1.366	O30-C32	1.385	1.390
C20-C25	1.395	1.395[44]	C31-C32	1.394	1.385
C21-C22	1.387	1.385	C33-C34	1.393	1.381
C22-C23	1.395	1.379	C31-C36	1.392	1.390
C23-C24	1.395	1.367	C34-C35	1.393	1.390
C23-O30	1.375	1.390[44]			

3.3.4 Bond Angles

Bond angles, which are frequently expressed in degrees, are any angles that exist between two bonds that have an atom in common. The outcomes of Table 3.2 and Figure 3.6 for the benzene rings (1, 2, and 3) show that the calculated average value of the first benzene ring bond angle was determined to be 119.5^0, which closely matched the practical value of 119.3^0. Similarly, the average of the second ring and the third ring bond angles was found, respectively, to be 119.9^0 and 120.1^0, which is closely related to the practical values of 119.9^0 and 119.8^0, respectively. In addition, the average values of the bond angles for the total rings are calculated to be 119.8^0 theoretically and 119.6^0 experimentally [39].

The theoretical values were found to agree well with the standard value, which is 120^0. The angles of the atoms in the benzene ring have similar values because they are in a similar environment. Short bond angles C6-C9-N11 and C1-C10-N11 in polyimide chains have been found to have values of 104.7° each. The lone pairs of the nitrogen atom cause this behavior because of the nitrogen atom's strong electronegativity. Since each nitrogen atom has two lone pairs, it has a higher electron density than a carbon atom. Table 3.2 shows the polyimide molecule's bond angle using DFT/B3LYP with 6-311G (d,p).

3.3.5 Dihedral Angle

A dihedral angle can be defined as the angle that exists between two planes, it involves four atoms, and its whole range is -180 to +180 degrees. When the molecule is rotated around its plane in a clockwise direction, the torsion angle is positive. When it is spun around its plane in an anticlockwise direction, it is negative. Typically, all of the hydrogen atoms in the benzene ring are sp2 hybridized, making them all trigonal planar with 120° bond angles.

For this work, the values of the dihedral angles of the benzene ring at C6-C1-C2-C3 and C10-C1-C6-C9 were all less than or equal to 0.01. Examples of dihedral angles with the greatest values include C10-C1-C2-C3, C2-C1-C10-N11, and C4-C3-C13=O19 due to the benzene ring's stiff atom connections. Because of their terminal position and single bond, the terminal dihedral angles C13-N14-C20-C21, C23-O30-C32-C31, and C15-N14-C20-C25 may spin readily.Table 3.3 shows the polyimide molecule's dihedral angles using DFT/B3LYP with 6-311G (d,p).

Table 3.2: Bond angles of PI in Degree unit.

Bond	Bond Angle	Experimental [39, 44]	Bond	Bond Angle	Experimental [39, 44]
N11-C10=O17	126.4	124.3	N14-C20-C21	120.2	
C9-N11-C10	113.7	111.2	N14-C20-C25	120.1	
C3-C13=O19	127.8	125.5	C21-C20-C25	119.8	120.0[44]
N14-C13=O19	126.4	124.3	C20-C21-C22	119.9	120.1
C13-N14-C15	111.5	111.2[44]	C22-C23-C24	120.1	119.7
C13-N14-C20	124.3		C22-C23-O30	116.2	119.60
C15-N14-C20	124.2		C23-O30-C32	120.9	
C4-C15-N14	105.8	105.9[44]	C32-C31-C36	119.2	118.4
N14-C15=O18	127.8	124.3[44]	O30-C32-C31	121.7	119.60
C2-C1-C6	122.5	119.8	C4-C5-C6	114.9	117.0[44]
C2-C1-C10	129.1	116.5	C1-C6-C5	122.5	119.8
C6-C1-C10	108.4	108.5	C1-C6-C9	108.4	108.5
C1-C2-C3	114.9	120.1	C5-C6-C9	129.6	123.7
C2-C3-C4	122.6	119.8	C6-C9-N11	104.7	105.9
C2-C3-C13	129.0	116.5	C6-C9=O16	128.8	125.5
C4-C3-C13	108.4	108.5	N11-C9=O16	126.4	124.3
C3-C4-C15	108.4	108.5[44]	C1-C10-N11	104.7	105.9
C5-C4-C15	129.0	123.7	C1-C10=O17	128. 9	124.3
C9-N11-C10	113.7	111.2	C32-C33-C34	119.5	120.0
C31-C32-C33	120.9	120.1	C34-C35-C36	119.7	120.0
C33-C34-C35	120. 3	120.1	O30-C32-C33	117.3	119.6
C34-C33-C35	120.5	120.1			

Table 3.3: Dihedral angles of PI in Degree units.

Angles	Dihedral	Angles	Dihedral Angles
C6-C1-C2-C3	-0.012	C2-C1-C10=O17	-0.009
C10-C1-C2-C3	-179.978	C6-C1-C10-N11	0.018
C2-C1-C6-C5	0.061	C6-C1-C10=O17	-179.979
C2-C1-C6-C9	-179.992	C1-C2-C3-C4	-0.093
C10-C1-C6-C5	-179.992	C1-C2-C3-C13	-179.908
C10-C1-C6-C9	-0.019	C2-C3-C4-C5	0.158
C2-C1-C10-N11	179.988	C2-C3-C4-C15	-179.995
C13-C3-C4-C5	-179.993	C2-C3-C13-N14	179.920
C13-C3-C4-C15	-0.147	C2-C3-C13=O19	-0.390
C4-C3-C13-N14	0.084	C4-C5-C6-C9	-179.938
C4-C3-C13=O19	179.774	C1-C6-C9-N11	0.0126
C3-C4-C5-C6	-0.102	C1-C6-C9=O16	-179.982
C15-C4-C5-C6	-179.914	C5-C6-C9-N11	179.954
C3-C4-C15-N14	0.154	C5-C6-C9=O16	-0.039
C3-C4-C15=O18	179.870	C6-C9-N11-C10	-0.0007
C5-C4-C15-N14	179.987	O16-C9-N11-C10	179.99
C5-C4-C15=O18	-0.297	C1-C10-N11-C9	-0.011
C4-C5-C6-C1	-0.004	O17=C10-N11-C9	179.987
C3-C13-N14-C15	0.016	C13-N14-C20-C21	-43.591
C3-C13-N14-C20	179.917	C20-N14-C15-C4	179.996
O19=C13-N14-C15	-179.679	C20-N14-	0.275
O19=C13-N14-C20	0.222	C13-N14-C20-C21	-43.591
C13-N14-C15-C4	-0.102	C13-N14-C20-C25	136.38
C13-N14-C15=O18	-179.823	C15-N14-C20-C21	136.298
C20-N14-C15=O18	0.275	C15-N14-C20-C25	-43.728
C13-N14-C20-C21	-43.607	N14-C20-C21-C22	-179.903
C13-N14-C15=O18	-179.823	C25-C20-C21-C22	0.123
C20-N14-C15=O18	0.275	C21-C20-C25-C24	-0.517
C20-C21-C22-C23	0.422	C36-C31-C32-C33	176.166
C21-C22-C23-C24	-0.577	C36-C31-C32-C33	0.601

C22-C23-C24-C25	0.184	C32-C31-C36-C35	-0.477
O30-C23-C24-C25	177.031	O30-C32-C33-C34	175.921
C22-C23-O30-C32	-156.006	C31-C32-C33-C34	-0.170
C24-C23-O30-C32	27.035	C32-C33-C34-C35	-0.391
C23-C24-C25-C20	0.362	C33-C34-C35-C36	0.531
C23-O30-C32-C31	53.825	C23-O30-C32-C33	-130.466
N14-C20-C25-C24	179.509	C34-C35-C36-C31	-0.074

3.3.6 Natural Bond Orbital (NBO) Charge Distribution

The importance of intermolecular orbital interaction particularly charge transfer in the complex is assured by NBO analysis. This is accomplished by taking into account all potential interactions [125]. In order to understand the outcomes of quantum chemical computations in a way that makes chemical, partial atomic charges are helpful descriptors. It all comes down to describing the distribution of electron charges inside molecules by giving each molecule's atom a partial charge.

Many alternative models have been developed to separate partial atomic charges from the molecular charge distribution since they are not accurately defined by quantum mechanics and are not physically observable. The models of partial atomic charges may be divided into many groups in theory [146]. This work uses a basis set of 6-311G (d, p) to explore the charge distribution of the PI according to the (NBO) charge distribution. This calculation shows the charges of each atom in the molecule. If the bond length between the atoms lengthens or shortens, it all depends on how the positive and negative charges are distributed. Table 4 lists the computed charges for the PI molecule.

The carbon atoms C31, C33, C34, C35, and C36 that are bonded to hydrogen atoms have comparable negative charges. Due to the coupled of the hydrogen atom with the carbon atom, C1, C3, C4, and C6 have somewhat different values

at the same moment. Because hydrogen may donate its electron, it is seen that all the hydrogen atoms in the molecule have positive charges and comparable values. Each of the carbon atoms C9, C10, C13, and C15 coupled to an oxygen atom has the largest positive value because the oxygen's electronegativity removes the electrons from the carbon atom, making it positive. While oxygen withholds, hydrogen atoms transfer electrons to the carbon atoms. Due to nitrogen's electronegativity, it is seen that every nitrogen atom in the molecule is negatively charged. The nitrogen atom, which is coupled to C20, has a positive value because of its ability to attract electrons from nearby carbon atoms. This charge distribution value indicates that the Mullikan method gives a minimum set value than the NBO method. The aim of using the Mullikan method is to compare and show the difference in the results as show Figure 3.7. Tables 3.4 and 3.5 show the polyimide molecule's atom charge using DFT/B3LYP with 6-311G(d,p).

Table 3.4: Natural bond orbital charges of PI.

Atom	Charges	Atom	Charges	Atom	Charges
C1	-0.098	C25	-0.175	H37	0.219
C2	-0.131	C31	-0.253	H38	0.217
C3	-0.090	C32	0.306	H39	0.204
C4	-0.090	C33	-0.237	H40	0.204
C5	-0.131	C34	-0.184	H41	0.204
C6	-0.098	C35	-0.214	N11	-0.652
C9	0.693	C36	-0.183	N14	-0.502
C10	0.693	H7	0.243	O16	-0.538
C13	0.704	H8	0.243	O17	-0.538
C15	0.704	H12	0.423	O18	-0.540
C20	0.120	H26	0.223	O19	-0,539
C21	-0.178	H27	0.220	O30	-0.528
C22	-0.231	H28	0.224		
C23	0.326	H29	0.222		

Table 3.5: Mullikan charges of PI.

| Atom	Charges	Atom	Charges	Atom	Charges
C1	-0.149	C25	-0.168	H37	0.219
C2	0.042	C31	-0.078	H38	0.217
C3	-0.134	C32	0.112	H39	0.215
C4	-0.134	C33	-0.079	H40	0.204
C5	0.042	C34	-0.094	H41	0.029
C6	-0.145	C35	-0.092	N11	-0.430
C9	0.432	C36	-0.096	N14	-0.540
C10	0.436	H7	0.126	O16	-0.289
C13	0.458	H8	0.126	O17	-0.283
C15	0.458	H12	0. 251	O18	-0.293
C20	0.143	H26	0.223	O19	-0.295
C21	-0.032	H27	0.220	O30	-0.357
C22	-0.093	H28	0.224		
C23	0.149	H29	0.222		
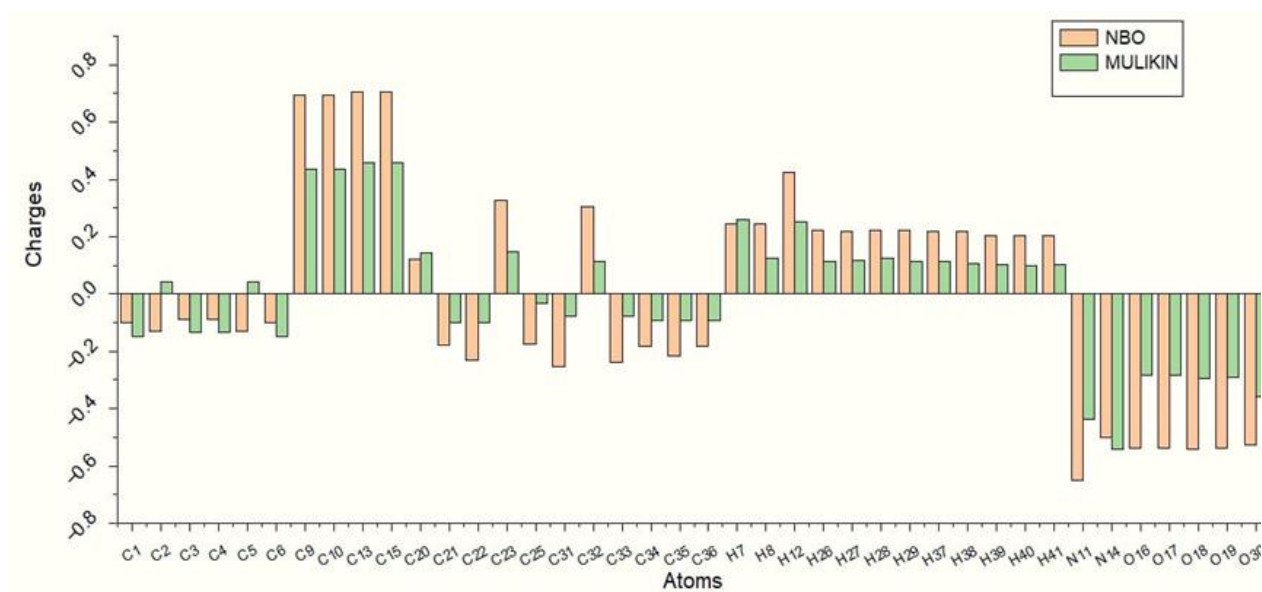
Figure 3.7: Comparison between charges using Mullikan and NBO charge distribution of PI.

3.4 Non-Linear Optical Properties

3.4.1 The Polarizability, First Order Hyperpolarizability and Susceptibility

Nonlinear optics is the study of light interaction with matter, where a material system responds nonlinearly to an applied electromagnetic field, producing new fields with altered frequency, phase, and amplitude [147].

The structures of polyimides have a major impact on their NLO properties, which include dipole moment, polarizability, and first-order polarizability values. The B3LYP method with the 6-311G(d,p) basis set was used to calculate these properties and their components. The acquired findings were convertedusing $\mathbf{1a.u.= 0.1482 * 10^{-24} esu}$ for α and $\mathbf{1a.u.= 8.6393 * 10^{-33}\ esu}$ for β to produce electronic units (esu).

For the PI, the nitrogen atom N14 has high electronegativity compared with the hydrogen H29 atom; therefore, a dipole moment was generated. Figure 3.6 shows that the arrow direction indicates the regions with higher electron density towards

the two benzene rings that are associated with a single oxygen atom. The dipoles of C15-O18 and C9-O16 will be cancelled by the dipoles of C13-O19 and C10-O17 because of the symmetry of the bonds of carbon and oxygen atoms in the dianhydride group PMDA. The average hyperpolarizability, anisotropy of polarizability and total dipole moment calculated using the DFT approach is displayed in Table 3.6. The values are 160.4518×10^{-33} esu, 259.1×10^{-24} esu, and 1.5253 Debye, respectively.

Higher dipole moment, molecule polarizability, and first-order hyperpolarizability values are known to be associated with more active NLO characteristics so when the average hyperpolarizability is 11 times greater than that of urea, it is deemed significant, the NLO system's molecular hyperpolarizability is a crucial component that must be considered. Furthermore, the mechanism of intermolecular charge transfer involves the sigma orbitals. The susceptibility was computed theoretically and compared with experimental values based on polarizability [51]. The values of the susceptibility are displayed in Table 3.7.

Table 3.6: The dipole moments, polarizability, and first hyperpolarizability of PI.

Parameter	B3LYP	Experimental value [51]
Dipole moment		
μ_x	1.1476	
μ_y	0.9832	
μ_z	-0.2071	
(Debye)μ	1.5253	
Polarizability in esu. ($* 10^{-24}$)		
a_{xx}	-148.7195	

a_{xy}	4.2149	
a_{yy}	-179.1569	
a_{xz}	-4.9315	
a_{yz}	-3.3318	
a_{zz}	-159.5560	
$\bar{a}$	-162.477	
$\Delta\alpha$	259.1	268.4

Hyperpolarizability in esu. ($*10^{-33}$)

β_{xxx}	64.8455
β_{xxy}	76.8194
β_{xyy}	89.5279
β_{yyy}	-7.8729
β_{xxz}	-49.3283
β_{xyz}	18.3788
β_{yyz}	10.0174
β_{xzz}	-14.1010
β_{yzz}	-3.3352
β_{zzz}	-2.6844
$\langle\beta\rangle$	160.4518

Table 3.7: The values for susceptibility of PI.

Parameter	PI
α'	$2.4 *10^{-24}$ m^3
Density	1.40 g/cm^3
N	$2.20 * 10^{27}$ m^{-3}
MW	382 g/mol
χ	0.25
χ (Theoretically) [51]	0.13

Where α': Polarizability volume, N: Molecular number density, M$_W$: Molar mass, and χ: Susceptibility.

The susceptibility value 0.25 indicates that the bonds are tightly connected, thus the electron is restricted in movement, which means that the material is an insulator.

The extracted values from the computational calculations, as shown in Table 3-6, for dipole moment, polarizability, first-order hyperpolarization, and optical susceptibility are exceedingly low. Which, in turn, indicates that the polyimide compound does not exhibit nonlinear optical properties.

Spectroscopy Properties

3.5.1 Vibrational Frequencies

In the case of nonlinear particles, the number of vibrational transitions is 3N-6 [148]. Because our molecule is made up of 41 atoms, it has 117 vibrational frequencies.

The molecule's mass and the strength of its bonds (constant of the bond force) determine the wavelength or frequency at which this absorption happens, as indicated by the equation below [149, 150]:

$$\eta = \frac{m_1 m_2}{m_1 + m_2} \qquad\qquad (3.1)$$

Where: m_1 and m_2 are the atomic mass for atoms 1 and 2 respectivity.

η: is the reduced mass.

$$v = \frac{1}{2\pi c}\sqrt{\frac{k}{\mu}} \qquad\qquad (3.2)$$

Where: **k** is the elasticity constant or the bond strength constant.

The DFT method was utilized to ascertain the PI's modes of vibration using B3LYP and a 6-311G (d, p) basis set. The obtained results have been compared with the experimental frequencies. Figure (3.8) displays the calculated IR spectrum through the [500–4000] cm^{-1} region after it was scaled by a factor of 0.9679, while Figure (3.9) shows the experimental values for the IR technique.

C-H Vibrations

Because of their aromatic C-H, aromatic compounds frequently show multiple weak bands in the 3100–3000 cm^{-1} region [151]. Nine C-H stretching vibrations were assigned in the current study. Figure 3.7 indicates that the C-H stretching vibrations calculated of the benzene ring are in the region (3065.6-3115.7) cm^{-1}. It is important to note that these stretching vibrations are not very strong in the infrared spectrum. They exhibit strong conformity with the specified experimental spectrum range of (2900–3100) cm^{-1} as shown in Figure 3.9 [41]. Since the benzene ring vibrations are observed at very similar wavenumbers in various compounds, assigning these vibrations is not too difficult.

Aromatic Ring Vibrations

In the vibrational spectra of benzene and its derivatives, the ring stretching vibrations are highly noticeable because the double bond is in conjugation with the ring [152]. The benzene ring vibrations are generally attributed to bands that appear in the range of (1400–1650) cm^{-1} [153]. The calculated C=C stretching

vibrations of benzene were detected in the range of (1436.9–1593.5) cm^{-1}. The experimental values of this mode were ranging from (1500–1520) cm^{-1} [154].

C=O and C-O-C Vibrations

Because carbon and oxygen have different electronegativity, a double bond between them is formed. The bonding electrons are not evenly distributed between the oxygen and carbon atoms; instead, they are more likely to be near the oxygen than the carbon atom. As a result, two poles will form, producing an important dipole moment and a strong C=O bond. The expected region for the C=O stretching mode is (1600–1750) cm^{-1}, and this vibration typically exhibits very strong peaks in this region [155]. At 1779.3 cm^{-1} and 1793.2 cm^{-1}, the stretching band of the C=O was observed. These values agree with the experimental values of 1770 cm^{-1} and 1780 cm^{-1}. The IR experimental values, which ranged from 1240 to 1270 cm^{-1} for C-O-C, agree well with the calculated values shown at 1245 cm^{-1} and 1280 cm^{-1}.

C-N and N-H Vibrations

Since multiple bands may mix in this area, identifying the C-N vibration is a challenging task. Typically, the C-N stretching vibration falls between 1200 cm^{-1} and 1400 cm^{-1} [156]. Within this current study, it is noted that there is a strong correlation between the experimental values at (1360–1380) cm^{-1} and the theoretically computed value at 1342.7 cm^{-1}. The stretching N-H mode at 3512.6 cm^{-1} is visible, and the values of the FT-IR experimental for it were 3400 cm^{-1} [41].
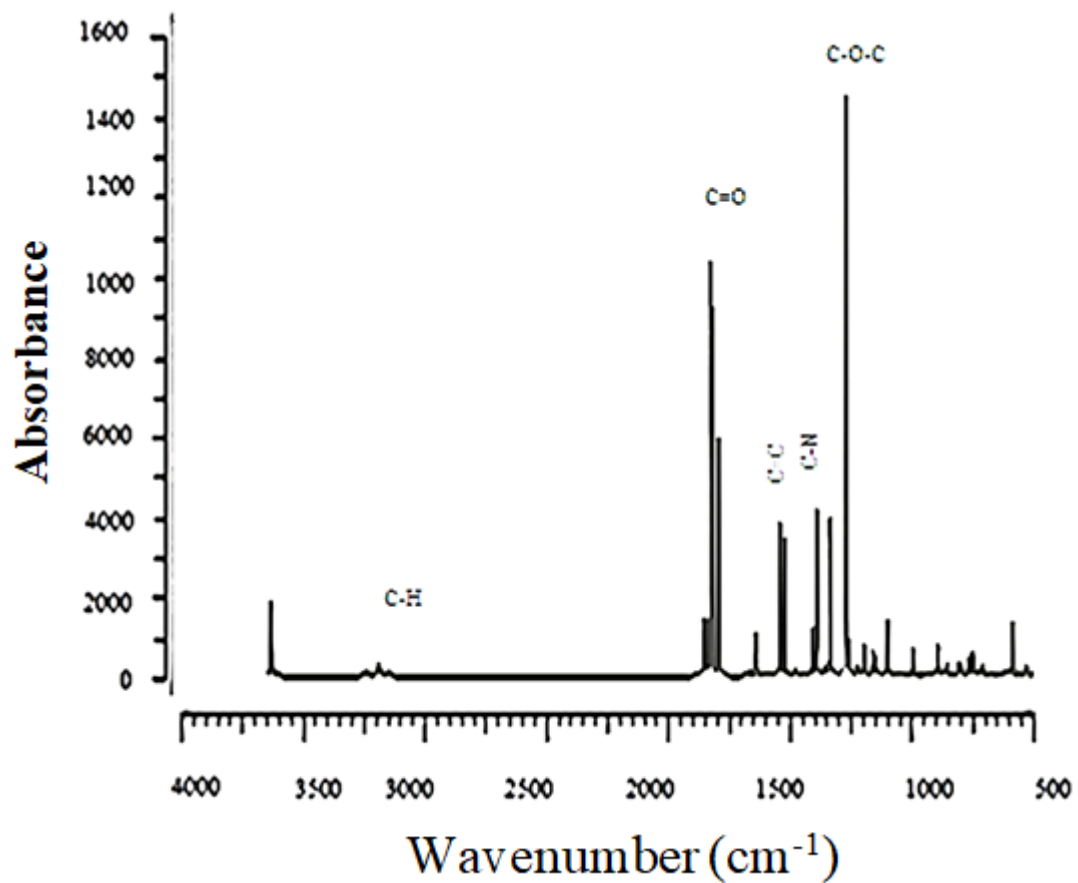
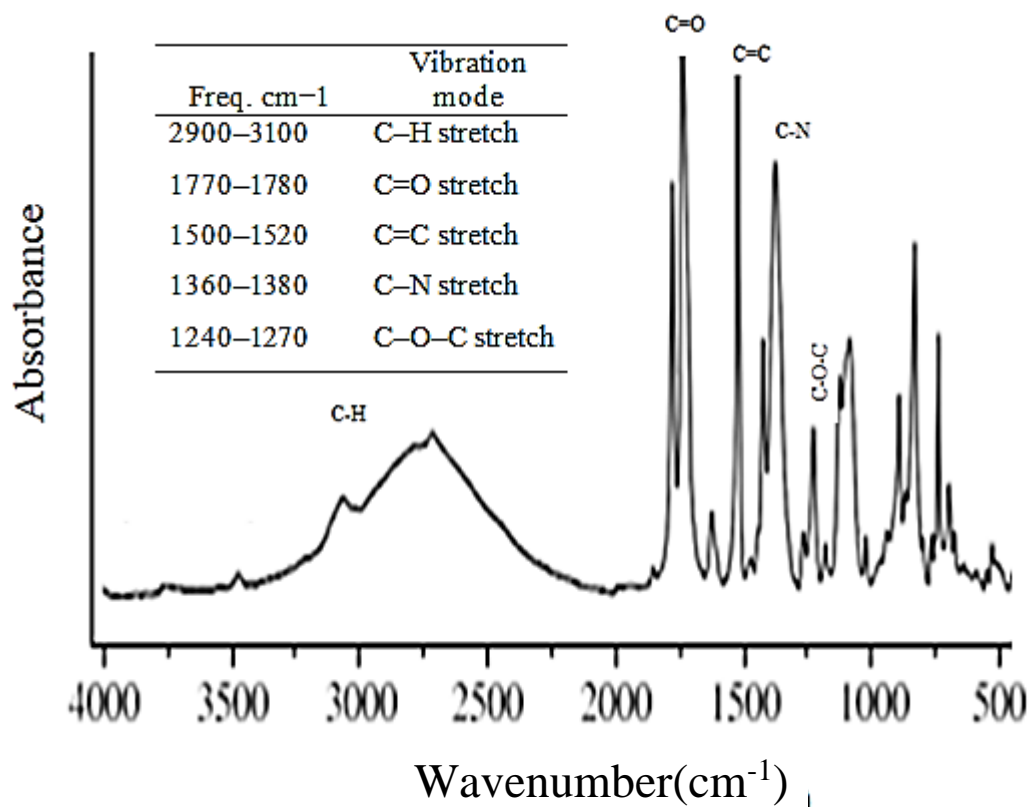**Figure 3.8: Theoretical IR absorption spectrum of PI using B3LYP.**

Figure 3.9: Experimental IR absorption spectrum of PI [41].

3.5.2 Ultraviolet (UV) Spectroscopy

Generally, it is believed that aromatic compounds (PIs) absorb UV light by forming a charge-transfer complex (CTC) between the dianhydride and the diamine, in which the latter serves as an electron acceptor and the former as an electron donor. As seen in Figure 3.11, PI exhibits nearly zero transmittance at wavelengths less than 480 nm, which is linked to $\pi–\pi^*$ transitions in the aromatic groups [157].

The optimized ground-state geometric monomer of the PI's theoretical UV spectrum has been investigated using the TD-B3LYP method with a 6-311G (d, p) basis set. In this study, the calculated wavelength appeared in the range of 300–1100 nm using UV technology as shown in Figure 3.10. The maximum wavelength at the oscillator strength (f = 0.0007) is 513 nm, see Table (3.8) and Figure (3.10). It has been noticed that these outcomes agree with the

experimental value of 500 nm [158]. The value of the longest wavelength 513 nm indicates that ultraviolet rays with a long wavelength are not considered ionizing radiation because the photon lacks energy. Since the majority of radiation is blocked by the eye's lens in the minimum wavelength range of 300–400 nm, polyimide is used in glass coating applications.

Table 3.8: Theoretical and experimental value of maximum wavelength of PI.

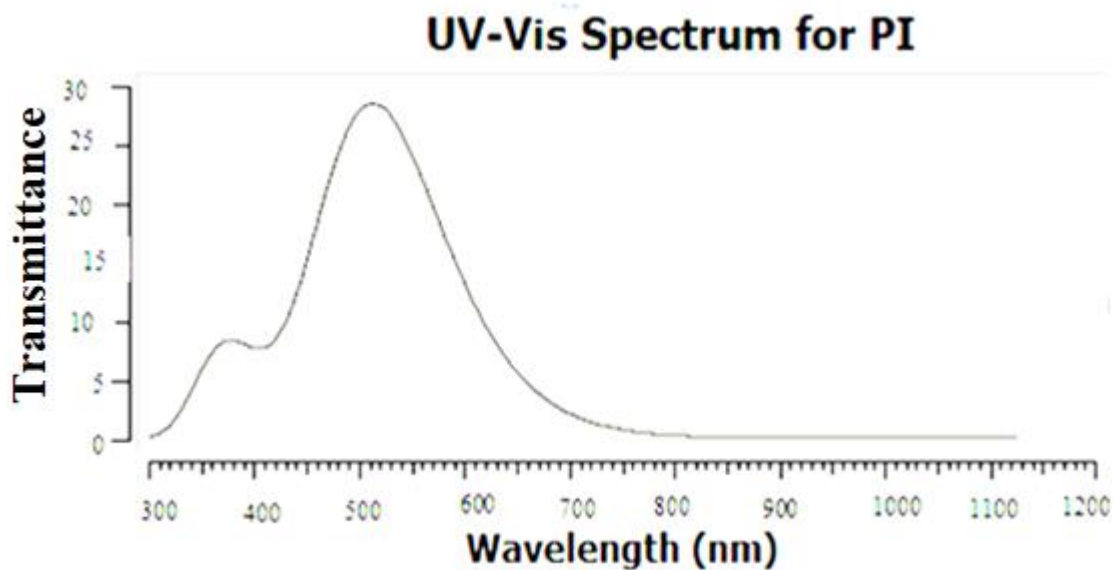| Theoretical λ_{max}(nm)		Experimental λ_{max} (nm) [158]
TD-B3LYP	513	500

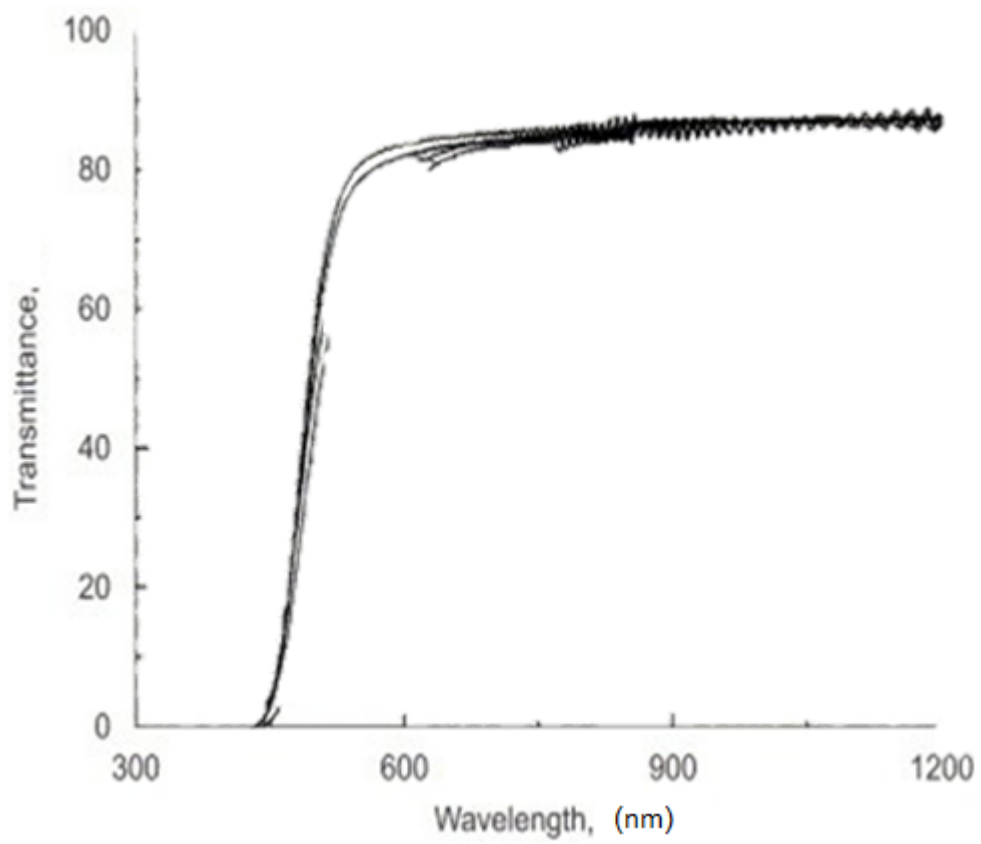**Figure 3.10: Theoretical UV spectrum of PI.**

Figure 3.11: Experimental UV spectrum of PI [158]**.**

3-6 Conclusion

In this work, the structural and NLO optical properties of the PI molecule have been examined using the density functional theory (B3LYP). The results were obtained with Gaussian 09 and visualized with Gauss View 06 and compared the results to the experimental values. Based on these findings, the following conclusions can be shown:

1. The potential energy surface scan technique is an effective and essential tool for preparing a molecule's geometry before fully optimizing it.

2. The results show that the bond lengths calculated at C9=O16, C15=O18, and C13=O19 are shorter than those of other bond lengths. This is due to the high negativity of oxygen and the double bonds responsible for this behavior.

3. Because of oxygen's high electronegativity, all of the oxygen atoms (O16, O17, O18, and O19) have comparable values and a negative charge.

4. The nitrogen atoms N11 and N14 constitute the lone pairs that give rise to the short bond angles C6-C9-N11, C4-C15-N14, and C1-C10-N11. They cause distorted angles, and an increase in electron density, and their lone pair of electrons exerts a stronger repulsive force compared to the bonding electrons

5. The ability of hydrogen to donate an electron is the reason why every hydrogen atom in the molecule is seen to be positive and has a similar value.

6. The results show that the charge distribution calculated using the NBO method is better than those found using the Mullikan method.

7. The dipole moment value of PI 1.52 Debye indicates that the charges on the various atoms in the molecule are not distributed uniformly.

8. The susceptibility value 0.2 indicates that the bonds are tightly connected, thus the electron is restricted in movement, which means that the material is an insulator.

9. We conclude that the polyimide compound does not exhibit nonlinear optical properties based on the very low values for dipole moment, polarizability, and first-order hyperpolarizability, as well as optical susceptibility.

10. The results of the IR techniques show that there is good agreement between the experimental and DFT-calculated results.

11. The value of the longest wavelength 513nm indicates that ultraviolet rays with a long wavelength are not considered ionizing radiation because the photon lacks energy. Each wavelength has a specific application for which it absorbs or blocks radiation through it.

3-7 Future Works

1- Investigation of the thermal and electronic properties of the polyimide using the DFT method.

 2- Use density functional theory to examine the impact of nano silica on the mechanical properties of polyimide/SiO2 composites.

References

[1] R. O. Ebewele, "POLYMER SCIENCE AND TECHNOLOGY," 2000.

[2] L. H. Sperling, *Introduction to physical polymer science*: John Wiley & Sons, 2005.

[3] C. S. Brazel and S. L. Rosen, *Fundamental principles of polymeric materials*: John Wiley & Sons, 2012.

[4] S. D. Bergman and F. Wudl, "Mendable polymers," *Journal of Materials Chemistry,* vol. 18, pp. 41-62, 2008.

[5] A. Ismail, D. Nasrallah, and E. El-Metwally, "Modulation of the optoelectronic properties of polyimide (Kapton-H) films by gamma irradiation for laser attenuation and flexible space structures," *Radiation Physics and Chemistry,* vol. 194, p. 110026, 2022.

[6] A. Sezer Hicyilmaz and A. Celik Bedeloglu, "Applications of polyimide coatings: A review," *SN Applied Sciences,* vol. 3, pp. 1-22, 2021.

[7] H. Ohya, V. Kudryavsev, and S. I. Semenova, *Polyimide membranes: applications, fabrications and properties*: Routledge, 2022.

[8] J. Q. Lin, J. Leng, M. H. Xia, J. H. Shi, and Q. G. Chi, "Polyimide electronic structural and optical properties from first principles calculations," in *Materials Science Forum*, 2011, pp. 597-601.

[9] C. Feger, *Advances in polyimide: science and technology*: CRC Press, 1993.

[10] M. Cen-Puc, A. Schander, M. G. Vargas Gleason, and W. Lang, "An assessment of surface treatments for adhesion of polyimide thin films," *Polymers,* vol. 13, p. 1955, 2021.

[11] D. Boll, K. Schubert, C. Brauner, and W. Lang, "Miniaturized flexible interdigital sensor for in situ dielectric cure monitoring of composite materials," *IEEE sensors journal,* vol. 14, pp. 2193-2197, 2014.

[12] T. Yang, Y. Yu, L. Zhu, X. Wu, X. Wang, and J. Zhang, "Fabrication of silver interdigitated electrodes on polyimide films via surface modification and ion-exchange technique and its flexible humidity sensor application," *Sensors and Actuators B: Chemical,* vol. 208, pp. 327-333, 2015.

[13] M. Hübner, D. Lepke, E. Hardi, M. Koerdt, A. S. Herrmann, and W. Lang, "Online monitoring of moisture diffusion in carbon fiber composites using miniaturized flexible material integrated sensors," *Sensors,* vol. 19, p. 1748, 2019.

[14] J. Engel, J. Chen, and C. Liu, "Development of polyimide flexible tactile sensor skin," *Journal of micromechanics and microengineering,* vol. 13, p. 359, 2003.

[15] F. Lin, W. Li, Y. Tang, H. Shao, C. Su, J. Jiang*, et al.*, "High-performance polyimide filaments and composites improved by O2 plasma treatment," *Polymers,* vol. 10, p. 695, 2018.

[16] H. Qu, Z. Wang, and D. Cang, "Flexible bandpass filter fabricated on polyimide substrate by surface modification and in situ self-metallization technique," *Polymers,* vol. 11, p. 2068, 2019.

[17] Y. J. Park, D. M. Yu, J. H. Ahn, J.-H. Choi, and Y. T. Hong, "Surface modification of polyimide films by an ethylenediamine treatment for a flexible copper clad laminate," *Macromolecular Research,* vol. 20, pp. 168-173, 2012.

[18] D. R. Cairns, D. J. Broer, and G. P. Crawford, *Flexible Flat Panel Displays*: John Wiley & Sons, 2023.

[19] D. J. Liaw and F. C. Chang, "Highly organosoluble and flexible polyimides with color lightness and transparency based on 2, 2-bis [4-(2-trifluoromethyl-4-aminophenoxy)-3, 5-dimethylphenyl] propane," *Journal of Polymer Science Part A: Polymer Chemistry,* vol. 42, pp. 5766-5774, 2004.

[20] A. Shiotani, H. Shimazaki, and M. Matsuo, "Preparation of Transparent Polyimides Derived from cis-and trans-Dicyclohexyl-3, 3', 4, 4'-tetracarboxylic Dianhydrides," *Macromolecular Materials and Engineering,* vol. 286, pp. 434-441, 2001.

[21] C. Lee, J. Seo, Y. Shul, and H. Han, "Optical properties of polyimide thin films. Effect of chemical structure and morphology," *Polymer journal,* vol. 35, pp. 578-585, 2003.

[22] J. C. Coburn, M. T. Pottiger, S. C. Noe, and S. D. Senturia, "Stress in polyimide coatings," *Journal of Polymer Science Part B: Polymer Physics,* vol. 32, pp. 1271-1283, 1994.

[23] A. Skontorp, "Strength and failure mechanisms of polyimide-coated optical fibers," in *Smart Structures and Materials 2000: Sensory Phenomena and Measurement Instrumentation for Smart Structures and Materials*, 2000, pp. 240-251.

[24] A. K. Dikshit, "Continuous flow of polyimide coating on silica optical fibre and its characterization," *International Journal of Plastics Technology,* vol. 20, pp. 401-423, 2016.

[25] Y. Zhang, L. Qu, J. Liu, X. Wu, Y. Zhang, R. Zhang*, et al.*, "Synthesis and characterization of high-temperature-resistant and optically transparent polyimide coatings for potential applications in quartz optical fibers protection," *Journal of Coatings Technology and Research,* vol. 16, pp. 511-520, 2019.

[26] E. Sugimoto, "Applications of polyimide films to the electrical and electronic industries in Japan," *IEEE Electrical Insulation Magazine,* vol. 5, pp. 15-23, 1989.

[27] H. Gao, X. Lan, L. Liu, X. Xiao, Y. Liu, and J. Leng, "Study on performances of colorless and transparent shape memory polyimide film in space thermal cycling, atomic oxygen and ultraviolet irradiation environments," *Smart Materials and Structures,* vol. 26, p. 095001, 2017.

[28] Y.-S. Hsiao, W.-T. Whang, S.-C. Wu, and K.-R. Chuang, "Chemical formation of palladium-free surface-nickelized polyimide film for flexible electronics," *Thin Solid Films,* vol. 516, pp. 4258-4266, 2008.

[29] N. Cherkashina, V. Pavlenko, V. Manaev, O. Kuprieva, N. Kashibadze, and E. Samoilova, "Multilayer coatings based on polyimide track membranes and nanodispersed lead," *Progress in Organic Coatings,* vol. 138, p. 105432, 2020.

[30] S. Diaham, *Polyimide for electronic and electrical engineering applications*: BoD–Books on Demand, 2021.

[31] X. Feng and R. Y. Huang, "Liquid separation by membrane pervaporation: a review," *Industrial & Engineering Chemistry Research,* vol. 36, pp. 1048-1066, 1997.

[32] P. Bernardo, E. Drioli, and G. Golemme, "Membrane gas separation: a review/state of the art," *Industrial & engineering chemistry research,* vol. 48, pp. 4638-4663, 2009.

[33] M. M. Pendergast and E. M. Hoek, "A review of water treatment membrane nanotechnologies," *Energy & Environmental Science,* vol. 4, pp. 1946-1971, 2011.

[34] H. Yanagishita, D. Kitamoto, K. Haraya, T. Nakane, T. Okada, H. Matsuda*, et al.*, "Separation performance of polyimide composite membrane prepared by dip coating process," *Journal of Membrane Science,* vol. 188, pp. 165-172, 2001.

[35] Y. H. Yu, J. M. Yeh, S. J. Liou, C. L. Chen, D. J. Liaw, and H. Y. Lu, "Preparation and properties of polyimide–clay nanocomposite materials for anticorrosion application," *Journal of applied polymer science,* vol. 92, pp. 3573-3582, 2004.

[36] S. T. Jolley, "Low-melt polyamic acid based powder coatings," 2017.

[37] M.-g. Huangfu, Y. Zhang, X.-l. Zhang, J.-g. Liu, Y.-c. Liu, Y.-d. Guo*, et al.*, "Preparation and thermal evaluation of novel polyimide protective coatings for quartz capillary chromatographic columns operated over 320 C for high-temperature gas chromatography analysis," *Polymers,* vol. 11, p. 946, 2019.

[38] S. Diaham, "Polyimide in electronics: Applications and processability overview," *Polyimide for Electronic and Electrical Engineering Applications,* pp. 2020-2021, 2021.

[39] N. Takahashi, D. Y. Yoon, and W. Parrish, "Molecular order in condensed states of semiflexible poly (amic acid) and polyimide," *Macromolecules,* vol. 17, pp. 2583-2588, 1984.

[40] M. M. Ramos, A. M. Stoneham, and A. P. Sutton, "Aluminium/polyimide adhesion," *Acta metallurgica et materialia,* vol. 41, pp. 2105-2111, 1993.

[41] S. Diaham, M.-L. Locatelli, T. Lebey, and D. Malec, "Thermal imidization optimization of polyimide thin films using Fourier transform infrared spectroscopy and electrical measurements," *Thin solid films,* vol. 519, pp. 1851-1856, 2011.

[42]   A. Abe, T. Nakano, W. Yamashita, K. Fukukawa, M. Okazaki, and S. Tamai, "Theoretical and experimental studies on the mechanism of coloration of polyimides," *ChemPhysChem,* vol. 12, pp. 1367-1377, 2011.

[43]   S. Lyulin, A. Gurtovenko, S. Larin, V. Nazarychev, and A. Lyulin, "Microsecond atomic-scale molecular dynamics simulations of polyimides," *Macromolecules,* vol. 46, pp. 6357-6363, 2013.

[44]   Y. Umar and S. Abdalla, "Experimental FTIR and Theoretical Investigation of the Molecular Sturcture and Vibrational Spectra of Terephthaloyl Chloride by Density Functional Theory," *IOSR Journal of Applied Chemistry (IOSR-JAC),* vol. 8, pp. 26-34, 2015.

[45]   A. Atta and S. El-Sayed, "Effect of oxygen plasma treatments on the structural and optical properties of polyimide films," *journal of Engineering and Technology Research,* vol. 7, pp. 10-12, 2015.

[46]   R. Mikšová, A. Macková, M. Cutroneo, P. Slepička, and J. Matoušek, "Compositional, structural and optical changes of polyimide irradiated by heavy ions," *Surface and Interface analysis,* vol. 48, pp. 566-569, 2016.

[47]   K.-H. Nam, H. Kim, H. K. Choi, H. Yeo, M. Goh, J. Yu*, et al.*, "Thermomechanical and optical properties of molecularly controlled polyimides derived from ester derivatives," *Polymer,* vol. 108, pp. 502-512, 2017.

[48]   S. Ando, M. Harada, T. Okada, and R. Ishige, "Effective reduction of volumetric thermal expansion of aromatic polyimide films by incorporating interchain crosslinking," *Polymers,* vol. 10, p. 761, 2018.

[49]   A. Rahnamoun, D. P. Engelhart, S. Humagain, H. Koerner, E. Plis, W. J. Kennedy*, et al.*, "Chemical dynamics characteristics of Kapton polyimide damaged by electron beam irradiation," *Polymer,* vol. 176, pp. 135-145, 2019.

[50]   C. Yang, R. Xu, S. Tang, Y. Zhuang, L. Luo, and X. Liu, "Free H-Bonding Interaction Sites in Rigid-Chain Polymers and Their Filling Approach: A Molecular Dynamics Simulation Study," *Advanced Theory and Simulations,* vol. 4, p. 2100016, 2021.

[51]   H. Lei, X. Li, J. Wang, Y. Song, G. Tian, M. Huang*, et al.*, "DFT and molecular dynamic simulation for the dielectric property analysis of polyimides," *Chemical Physics Letters,* vol. 786, p. 139131, 2022.

[52]   J. Tan, F. Xie, J. Huang, X. Liu, H. Li, J. Yuan*, et al.*, "Design and synthesis of intrinsic black polyimide with full visible-light absorption and low coefficient of thermal expansion for black flexible copper clad laminates," *Polymer Testing,* vol. 129, p. 108247, 2023.

[53]   A. Raluca Marinica, L. I. BURUIANA, I. STOICA, C. HULUBEI, and A. I. BARZIC, "DIANHYDRIDE MOIETIES INVOLVEMENT ON THE INTERACTIONS OF SOME POLYIMIDES WITH NEMATIC COMPOUNDS," *Rev. Roum. Chim,* vol. 68, pp. 227-232, 2023.

[54]   J. Luo, H. Tong, S. Mo, F. Zhou, S. Zuo, C. Yin*, et al.*, "Integrated exploration of experimentation and molecular simulation in ester-containing polyimide dielectrics," *RSC advances,* vol. 13, pp. 963-972, 2023.

[55]   J. A. Pople and D. L. Beveridge, "Molecular orbital theory," *C0., NY,* 1970.

[56]   H. F. Hameka, *Quantum mechanics: a conceptual approach*: John Wiley & Sons, 2004.

[57]   F. A. Berezin and M. Shubin, *The Schrödinger Equation* vol. 66: Springer Science & Business Media, 2012.

[58]   D. J. Tannor, N. Takemoto, and A. Shimshovitz, "Phase space approach to solving the Schrödinger equation: Thinking inside the box," *Advances in Chemical Physics,* vol. 156, pp. 1-34, 2014.

[59]   H. Spohn and S. Teufel, "Adiabatic decoupling and time-dependent Born–Oppenheimer theory," *Communications in Mathematical Physics,* vol. 224, pp. 113-132, 2001.

[60]   S. Takeuchi, M. Iida, S. Kobayashi, K. Jin, T. Matsuda, and H. Kojima, "Differential effects of phthalate esters on transcriptional activities via human estrogen receptors α and β, and androgen receptor," *Toxicology,* vol. 210, pp. 223-233, 2005.

[61]   D. W. Rogers, *Computational Chemistry using the PC*: John Wiley & Sons, 2003.

[62]   R. Gobato and A. Heidari, "Infrared Spectrum and Sites of Action of Sanguinarine by Molecular Mechanics and ab initio Methods"," *mechanics,* vol. 30, p. 34, 2018.

[63]   E. G. Lewars, "Computational chemistry," *Introduction to the theory and applications of molecular and quantum mechanics,* vol. 318, 2011.

[64]   M. J. Morris, "Size-exclusion chromatography with refractometric and viscometric detection to determine the solution conformational entropy of mono-, di-, and oligosaccharides," The Florida State University, 2013.

[65]   J. J. Stewart, "Optimization of parameters for semiempirical methods IV: extension of MNDO, AM1, and PM3 to more main group elements," *Journal of Molecular Modeling,* vol. 10, pp. 155-164, 2004.

[66]   J. J. Stewart, "Optimization of parameters for semiempirical methods II. Applications," *Journal of computational chemistry,* vol. 10, pp. 221-264, 1989.

[67]   W. Thiel and A. A. Voityuk, "Extension of MNDO to d Orbitals: Parameters and Results for the Second-Row Elements and for the Zinc Group," *The Journal of Physical Chemistry,* vol. 100, pp. 616-626, 1996.

[68]   M. J. Dewar, E. G. Zoebisch, E. F. Healy, and J. J. Stewart, "Development and use of quantum mechanical molecular models. 76. AM1: a new general purpose quantum mechanical molecular model," *Journal of the American Chemical Society,* vol. 107, pp. 3902-3909, 1985.

[69]   R. Latour, "3.14 molecular simulation methods to investigate protein adsorption behavior at the atomic level," 2017.

[70]   J. Pokluda, M. Černý, M. Šob, and Y. Umeno, "Ab initio calculations of mechanical properties: Methods and applications," *Progress in Materials Science,* vol. 73, pp. 127-158, 2015.

[71]   P. Dağtepe, *A computational study on the structure of allene polymers by using quantum chemical methods*: Izmir Institute of Technology (Turkey), 2005.

[72]   H. B. Jasim, "Theoretical and Experimental Study For (CdSe) Nanoparticles," University of Baghdad, 2014.

[73]   A. K. Sachan, "Applications of ab initio quantum chemistry to small organic molecules," Ph. D. thesis, University of Lucknow, India, 2015.

[74]   A. K. Sachan, "Applications of ab initio quantum chemistry to small organic molecules," 2015.

[75]   F. Schwabl, *Quantum mechanics*: Springer Science & Business Media, 2007.

[76]   M. Ghaedi, *Photocatalysis: fundamental processes and applications*: Academic Press, 2021.

[77]   A. Szabo and N. S. Ostlund, *Modern quantum chemistry: introduction to advanced electronic structure theory*: Courier Corporation, 2012.

[78]   D. C. Young, "A practical guide for applying techniques to real-world problems," *Computational Chemistry, New York,* vol. 9, p. 390, 2001.

[79]   H. Eschrig, *The fundamentals of density functional theory* vol. 32: Springer, 1996.

[80]   W. Koch and M. C. Holthausen, *A chemist's guide to density functional theory*: John Wiley & Sons, 2015.

[81]   R. G. Parr, "Density functional theory," *Annual Review of Physical Chemistry,* vol. 34, pp. 631-656, 1983.

[82]   A. J. Cohen, P. Mori-Sánchez, and W. Yang, "Challenges for density functional theory," *Chemical reviews,* vol. 112, pp. 289-320, 2012.

[83]   P. Hohenberg and W. Kohn, "Inhomogeneous electron gas," *Physical review,* vol. 136, p. B864, 1964.

[84]   W. Kohn and L. J. Sham, "Self-consistent equations including exchange and correlation effects," *Physical review,* vol. 140, p. A1133, 1965.

[85]   H. A. Rashed and N. M. Umran, "The stability and electronic properties of Si-doped ZnO nanosheet: a DFT study," *Materials Research Express,* vol. 6, p. 045044, 2019.

[86]   J. Owolabi, M. Onimisi, S. Abdu, and G. Olowomofe, "Determination of band structure of gallium-arsenide and aluminium-arsenide using density functional theory," *Computational*

chemistry, vol. 4, pp. 73-82, 2016.

[87] Y. Shi and A. Wasserman, "Inverse Kohn–Sham density functional theory: Progress and challenges," *The journal of physical chemistry letters,* vol. 12, pp. 5308-5318, 2021.

[88] E. Acheampong, "Computational Quantum Chemistry Studies of the Interactions of Amino Acids Side Chains with the Guanine Radical Cation," East Tennessee State University, 2018.

[89] D. Zhou, "An introduction of Density Functional Theory and its application," *Physics. Drexel. Edu,* 2007.

[90] O. A. A. Al-Owaedi, *Electronic properties of nano and molecular quantum devices*: Lancaster University (United Kingdom), 2016.

[91] F. Brockherde, L. Vogt, L. Li, M. E. Tuckerman, K. Burke, and K.-R. Müller, "Bypassing the Kohn-Sham equations with machine learning," *Nature communications,* vol. 8, p. 872, 2017.

[92] M. H. Cohen, D. Frydel, K. Burke, and E. Engel, "Total energy density as an interpretative tool," *The Journal of Chemical Physics,* vol. 113, pp. 2990-2994, 2000.

[93] J. Weis, H. Schäfer, and G. Schön, "Neue ternäre Telluride und Selenide der Alkalimetalle mit Elementen der 3. Hauptgruppe," 1976.

[94] R. M. Dreizler and E. K. Gross, *Density functional theory: an approach to the quantum many-body problem*: Springer Science & Business Media, 2012.

[95] K. Capelle, "A bird's-eye view of density-functional theory," *Brazilian journal of physics,* vol. 36, pp. 1318-1343, 2006.

[96] A. A. D. Al-Jobory, *Theory of electron transport through single molecules*: Lancaster University (United Kingdom), 2018.

[97] J. P. Perdew and A. Zunger, "Self-interaction correction to density-functional approximations for many-electron systems," *Physical Review B,* vol. 23, p. 5048, 1981.

[98] J. P. Perdew and S. Kurth, "Density functionals for non-relativistic Coulomb systems in the new century," in *A primer in density functional theory*, ed: Springer, 2003, pp. 1-55.

[99] M. L. Winterrose, *Quantum Mechanical Simulation and X-Ray Scattering Applied to Pressure-Induced Invar Anomaly in Magnetic Iron Alloy*: California Institute of Technology, 2011.

[100] M. Marsman, J. Paier, A. Stroppa, and G. Kresse, "Hybrid functionals applied to extended systems," *Journal of Physics: Condensed Matter,* vol. 20, p. 064201, 2008.

[101] R. L. Johnston, "Evolving better nanoparticles: Genetic algorithms for optimising cluster geometries," *Dalton Transactions,* pp. 4193-4207, 2003.

[102] N. Issaoui, K. Abdessalem, H. Ghalla, S. J. Yaghmour, F. Calvo, and B. Oujia, "Theoretical investigation of the relative stability of Na+ Hen (n= 2–24) clusters: Many-body versus delocalization effects," *The Journal of Chemical Physics,* vol. 141, 2014.

[103] A. D. Becke, "Density functional calculations of molecular bond energies," *The Journal of Chemical Physics,* vol. 84, pp. 4524-4529, 1986.

[104] C. Lee, W. Yang, and R. G. Parr, "Development of the Colle-Salvetti correlation-energy formula into a functional of the electron density," *Physical review B,* vol. 37, p. 785, 1988.

[105] O. Adnanhatem, F. S. A. Suhail, and A. M. Juda, "Optimized programs and methods required for the computational study of beta blockers," in *Journal of Physics: Conference Series*, 2020, p. 012088.

[106] M. M. Kadhim and R. M. Kubba, "Theoretical investigation on reaction pathway, biological activity, toxicity and NLO properties of diclofenac drug and its ionic carriers," *Iraqi Journal of Science,* pp. 936-951, 2020.

[107] M. Frisch Gwt, H. Schlegel, G. Scuseria, M. Robb, J. Cheeseman, G. Scalmani*, et al.*, "Gaussian 09, Revision A. 01," ed: Wallingford CT: Gaussian, Inc, 2016.

[108] R. Dennington, T. A. Keith, and J. M. Millam, "GaussView, version 6.0. 16," *Semichem Inc Shawnee Mission KS,* 2016.

[109] T. A. Julboev, M. M. Sultonov, and K. Abduvaliyeva, "Teaching Chemistry computer software to students of chemistry in pedagogical higher education institutions," *European Journal of Research and Reflection in Educational Sciences,* vol. 9, 2021.

[110] F. Jensen, "Atomic orbital basis sets," *Wiley Interdisciplinary Reviews: Computational Molecular Science,* vol. 3, pp. 273-295, 2013.

[111] A. C. Slov, "Book Review: Exploring Chemistry with Electronic Structure Methods, James B. Foresman and AEleen Frisch. Published by Gaussian, Inc., Pittsburgh, PA, 15106 USA. 354 pages. Soft cover: $42.00 ISBN 0-9636769-3-8, Hard cover: $100.00 ISBN 0-9636769-4-6 Abraham F. Jalbout," *Acta Chim. Slov,* vol. 50, pp. 159-160, 2003.

[112] J. A. R. Sandberg, *New efficient integral algorithms for quantum chemistry*: Biotechnology, KTH Royal Institute of Technology, 2014.

[113] J. Reel, "A comparative review of computational methods as applied to gold (I) complexes and mechanisms," Duke University, 2016.

[114] P. Duffy, D. P. Chong, M. E. Casida, and D. R. Salahub, "Assessment of Kohn-Sham density-functional orbitals as approximate Dyson orbitals for the calculation of electron-momentum-spectroscopy scattering cross sections," *Physical Review A,* vol. 50, p. 4707, 1994.

[115] E. R. Davidson and D. Feller, "Basis set selection for molecular calculations," *Chemical Reviews,* vol. 86, pp. 681-696, 1986.

[116] J. Foresman and E. Frish, "Exploring chemistry," *Gaussian Inc., Pittsburg, USA,* vol. 21, 1996.

[117] C. Zener, "Analytic atomic wave functions," *Physical Review,* vol. 36, p. 51, 1930.

[118] J. C. Slater, "Atomic shielding constants," *Physical review,* vol. 36, p. 57, 1930.

[119] T. Özdoğan, "Higher electric multipole moments for some polyatomic molecules from accurate SCF calculations," *Communications in Theoretical Physics,* vol. 38, p. 489, 2002.

[120] A. Yariv, *Quantum electronics*: John Wiley & Sons, 1989.

[121] A. Faure, J. D. Gorfinkiel, L. A. Morgan, and J. Tennyson, "GTOBAS: fitting continuum functions with Gaussian-type orbitals," *Computer physics communications,* vol. 144, pp. 224-241, 2002.

[122] P. E. Hoggan, M. B. Ruiz, and T. Özdogan, "Molecular integrals over slater-type orbitals. From pioneers to recent developments," *Quantum Frontiers ofAtoms and Molecules,* pp. 64-90, 2011.

[123] İ. Sıdır, Y. G. Sıdır, M. Kumalar, and E. Taşal, "Ab initio Hartree–Fock and density functional theory investigations on the conformational stability, molecular structure and vibrational spectra of 7-acetoxy-6-(2, 3-dibromopropyl)-4, 8-dimethylcoumarin molecule," *Journal of Molecular Structure,* vol. 964, pp. 134-151, 2010.

[124] V. Balachandran and K. Parimala, "Tautomeric purine forms of 2-amino-6-chloropurine (N9H10 and N7H10): Structures, vibrational assignments, NBO analysis, hyperpolarizability, HOMO–LUMO study using B3 based density functional calculations," *Spectrochimica Acta Part A: Molecular and Biomolecular Spectroscopy,* vol. 96, pp. 340-351, 2012.

[125] R. Gangadharan and S. Sampath Krishnan, "Natural Bond Orbital (NBO) population analysis of 1-azanapthalene-8-ol," *Acta Physica Polonica A,* vol. 125, pp. 18-22, 2014.

[126] M. Miar, A. Shiroudi, K. Pourshamsian, A. R. Oliaey, and F. Hatamjafari, "Theoretical investigations on the HOMO–LUMO gap and global reactivity descriptor studies, natural bond orbital, and nucleus-independent chemical shifts analyses of 3-phenylbenzo [d] thiazole-2 (3 H)-imine and its para-substituted derivatives: Solvent and substituent effects," *Journal of Chemical Research,* vol. 45, pp. 147-158, 2021.

[127] L. Sinha, M. Karabacak, V. Narayan, M. Cinar, and O. Prasad, "Molecular structure, electronic properties, NLO, NBO analysis and spectroscopic characterization of Gabapentin with experimental (FT-IR and FT-Raman) techniques and quantum chemical calculations," *Spectrochimica Acta Part A: Molecular and Biomolecular Spectroscopy,* vol. 109, pp. 298-307, 2013.

[128] N. Tsutsumi, M. Morishima, and W. Sakai, "Nonlinear optical (NLO) polymers. 3. NLO polyimide with dipole moments aligned transverse to the imide linkage," *Macromolecules,* vol. 31, pp. 7764-7769, 1998.

[129] J. Foresman and A. Frisch, "Exploring chemistry with electronic structure methods, 3rd edn. Wallingford, CT, USA: Gaussian," ed: Inc, 2015.

[130] D. Habibi, A. R. Faraji, D. Sheikh, M. Sheikhi, and S. Abedi, "Application of supported Mn (III), Fe (III) and Co (II) as heterogeneous, selective and highly reusable nano catalysts for synthesis of arylaminotetrazoles, and DFT studies of the products," *RSC Advances,* vol. 4, pp. 47625-47636, 2014.

[131] P. D. Kirsch, P. Sivasubramani, J. Huang, C. Young, M. Quevedo-Lopez, H. Wen*, et al.*, "Dipole model explaining high-k/metal gate field effect transistor threshold voltage tuning," *Applied Physics Letters,* vol. 92, 2008.

[132] S. Ramalingam, M. Karabacak, S. Periandy, N. Puviarasan, and D. Tanuja, "Spectroscopic (infrared, Raman, UV and NMR) analysis, Gaussian hybrid computational investigation (MEP maps/HOMO and LUMO) on cyclohexanone oxime," *Spectrochimica Acta Part A: Molecular and Biomolecular Spectroscopy,* vol. 96, pp. 207-220, 2012.

[133] Y. Zhang and W. Huang, "Soluble and Low-κ Polyimide Materials," in *Advanced Polyimide Materials*, ed: Elsevier, 2018, pp. 385-463.

[134] M. Asghari-Khiavi, P. Hojati-Talemi, and F. Safinejad, "Polarizability and first-order hyperpolarizability of cyclic imides," *Journal of Molecular Structure: THEOCHEM,* vol. 910, pp. 56-60, 2009.

[135] S. Sindhu, S. Muthu, M. Raja, and R. R. Muhamed, "Molecular structure, first order hyperpolarizability, NBO and HOMO-LUMO analysis of cinnoline-4-carboxylic acid," *Int. J. Adv. Scientific Technologies in Eng. Manage. Sci.,* vol. 3, p. 2454, 2017.

[136] F. Yao, C. Liu, C. Chen, S. Zhang, Q. Zhao, F. Xiao*, et al.*, "Measurement of complex optical susceptibility for individual carbon nanotubes by elliptically polarized light excitation," *Nature communications,* vol. 9, p. 3387, 2018.

[137] S. Hokenek, "Characterization of conductive polycarbonate films," 2009.

[138] B. C. Smith, *Infrared spectral interpretation: a systematic approach*: CRC press, 2018.

[139] K. Hashimoto, V. R. Badarla, A. Kawai, and T. Ideguchi, "Complementary vibrational spectroscopy," *Nature Communications,* vol. 10, p. 4411, 2019.

[140] R. Silverstien, F. Webster, and D. Kiemle, "Spectrometric Identification of Organic Compounds, 2005," ed: John Wiley and Sons, New Yourk, USA.

[141] S. A. Ghulam, M. AL-Kaabi, and W. S. Rasool, "Theoretical study of diallyl phthalate using density functional theory," in *AIP Conference Proceedings*, 2022.

[142] S. Chand, F. A. Al-Omary, A. A. El-Emam, V. K. Shukla, O. Prasad, and L. Sinha, "Study on molecular structure, spectroscopic behavior, NBO, and NLO analysis of 3-methylbezothiazole-2-thione," *Spectrochimica Acta Part A: Molecular and Biomolecular Spectroscopy,* vol. 146, pp. 129-141, 2015.

[143] S. Ruchi, "Quantum chemical and spectroscopic studies of some small systems."

[144] Y. Hu, L. Zuo, J. Liu, J. Sun, and S. Wu, "Chemical simulation and quantum chemical calculation of lignin model compounds," *BioResources,* vol. 11, pp. 1044-1060, 2016.

[145] D. R. Lide Jr, "A survey of carbon-carbon bond lengths," *Tetrahedron,* vol. 17, pp. 125-134, 1962.

[146] P. Matczak, "A test of various partial atomic charge models for computations on diheteroaryl ketones and thioketones," *Computation,* vol. 4, p. 3, 2016.

[147] S. Saravanan and V. Balachandran, "Quantum mechanical study and spectroscopic (FT-IR, FT-Raman, UV–Visible) study, potential energy surface scan, Fukui function analysis and HOMO–LUMO analysis of 3-tert-butyl-4-methoxyphenol by DFT methods," *Spectrochimica Acta Part A: Molecular and Biomolecular Spectroscopy,* vol. 130, pp. 604-620, 2014.

[148] M. Raja, R. R. Muhamed, S. Muthu, and M. Suresh, "Synthesis, spectroscopic (FT-IR, FT-Raman, NMR, UV–Visible), first order hyperpolarizability, NBO and molecular docking study of (E)-1-(4-bromobenzylidene) semicarbazide," *Journal of Molecular Structure,* vol. 1128, pp. 481-492, 2017.

[149] F. Rouessac, A. Rouessac, and D. Cruch??, *Analyse chimique*: Dunod, 2004.

[150] C. NAGAMOUTTOU, "Traitement thermique et caractérisation physicochimique de matériau

carbonés," *Rapport de stage, Centre de recherche sur la matière divisé, Université d'Orléans,* 2006.

[151] T. Cairns, I. G. McWilliam, R. L. Pecsok, and L. D. Shields, *Modern methods of chemical analysis. Pecsok*: John Wiley & Sons, 1976.

[152] G. Varsányi, *Vibrational spectra of benzene derivatives*: Elsevier, 2012.

[153] B. Amul, S. Muthu, M. Raja, and S. Sevvanthi, "Spectral, DFT and molecular docking investigations on Etodolac," *Journal of Molecular Structure,* vol. 1195, pp. 747-761, 2019.

[154] A. Altun, K. Gölcük, and M. Kumru, "Structure and vibrational spectra of p-methylaniline: Hartree-Fock, MP2 and density functional theory studies," *Journal of Molecular Structure: THEOCHEM,* vol. 637, pp. 155-169, 2003.

[155] F. Barbet, D. Bormann, M. Warenghem, B. Khelifa, Y. Kurios, Y. Reznikov*, et al.*, "Comparative Raman spectroscopy studies of photosensitive polymers," *Materials chemistry and physics,* vol. 55, pp. 202-208, 1998.

[156] M. Boopathi, P. Udhayakala, G. Ramkumaar, and T. R. Devi, "ISSN 0975-413X CODEN (USA): PCHHAX."

[157] J. P. LaFemina, G. Arjavalingam, and G. Hougham, "Electronic structure and ultraviolet absorption spectrum of polyimide," *The Journal of chemical physics,* vol. 90, pp. 5154-5160, 1989.

[158] E. A. Plis, D. P. Engelhart, R. Cooper, W. R. Johnston, D. Ferguson, and R. Hoffmann, "Review of radiation-induced effects in polyimide," *Applied Sciences,* vol. 9, p. 1999, 2019.

الخلاصة

في هذه الدراسة، تم إجراء حسابات نظرية الكثافة الوظيفية لدراسة الخصائص التركيبية والخصائص البصرية غير الخطية (NLO) والتحليل الطيفي لمونومر البولي مايد. تم إجراء مسح سطح الطاقة الكامنة (PES) باستخدام الطريقة شبه التجريبية PM6 للتنبؤ بأفضل شكل للمونومر. وقد تم استخدام الدالة B3LYP، التي تستخدم وظيفة التبادل الهجين ثلاثية المعلمات لـ Beck ووظيفة الارتباط Lee-Yang-Parr، و6-311G(d,p) بشكل فعال لتحسين المونومر وتقييم الخصائص. لقد تبين أن متوسط القيمة المحسوبة لأطوال الروابط لحلقة البنزين هو 1.392 بوحدات الانجستروم ، في حين أن متوسط قيمة زوايا الرابطة هو 119.8 درجة. ان أطوال وزوايا الاواصر التي تم الحصول عليها من نظرية الكثافة الوظيفية كانت متوافقة بصورة جيدة مع النتائج التجريبية.

تمت أيضًا دراسة توزيع الشحنات باستخدام طريقة(NBO) ، والخصائص البصرية اللاخطية مثل عزم ثنائي القطب والاستقطاب وفرط الاستقطاب من الدرجة الأولى وكذلك التاثرية. أدى ملاحظة التوزيع غير المتساوي للشحنات إلى عزم ثنائي القطب غير صفري قدره 1.52ديباي.

وأخيرا، تم الحصول على طيف الأشعة تحت الحمراء وتحليله بعد استخدام معامل قياس قدره 0.9679. كذلك تمت دراسة طيف امتصاص الأشعة فوق البنفسجية باستخدام طريقة TD-B3LYP وبنفس مجموعة الأساس. وقد وجد أن الطول الموجي الأقصى عند قوة المذبذب (f = 0.0007) هو 513 نانومتر وهو ما يتوافق بصورة جيدة مع القيمة العملية والمساوية لـ 500 نانومتر.

جامعة كـربلاء

كليــة العلـوم

قسم الفيزياء

استقصاء الخصائص التركيبية والبصرية اللاخطية للبوليمايد باستخدام نظرية دالة الكثافة الوظيفية

من قبل

زينب عادل احمد

بكالوريوس علوم في الفيزياء جامعة كربلاء

2011

بإشراف

أ.م. د. محمد عبدالحسين   د. قاسم حسن عبيد الكعبي

1446 هـ   2024 م